Diplomarbeit

Particle-in-cell (PIC) Simulation of the Plasma Sheath and Presheath Including Collisions and Secondary Electrons

Günther Eibl

eingereicht im November 2004
bei tit.ao. Univ-Prof. Dr. Siegbert Kuhn
Universität Innsbruck
Institut für Theoretische Physik

Contents

Acknowledgement

First I would like to thank Professor S. Kuhn. At his plasma theory and simulation group I could explore how simulations are done in plasma physics. He also made it possible for me to stay abroad in order to learn more about plasma physics and particularly about fusion physics.

I would especially like to thank Dr. David Tskhakaya, who showed me how to make proper simulations. In addition, I learned from his personal example how important it is to not only correctly set some simulation parameters but to also have a broad physical knowledge.

I would like to thank Mag. Steluta Teodoru for giving me advice especially the first times I made particle simulations.

I had many nice lunch breaks with Mag. Anton Schneider who, in addition to physics discussions, amused me with his many interests such as foreign (=Vorarlberg) customs and languages.

Finally I would like to thank all my family members and friends, who supported me during my whole life.

Abstract

In this thesis the influence of secondary electrons on the stability of the presheath is investigated. Secondary electrons are emitted from the wall due to the impact of primary particles. They get accelerated by the sheath potential and enter the presheath essentially as a cold beam. If the corresponding electron-beam instability is stronger than the damping processes in the presheath, the presheath becomes unstable. The approximate theoretical treatment of this problem mainly includes the derivation of the dispersion relation. The numerical solution of the dispersion relation shows that we can expect an instability induced by the secondary electrons. The problem is also treated by means of Particle-in-cell (PIC) simulations, where the instability induced by the secondary electrons is observed as well. In addition to these already known results we propose a mechanism which saturates the instability. As the (initially cold) secondary electron beam enters the presheath, its temperature rises. This temperature rise has the effect that the minimum in the total electron velocity distribution gets so shallow, that the instability criterion of Penrose is not fulfilled any more. Further investigations will include a theoretical treatment where the secondary electrons are no longer treated as a cold beam. Additional simulations will be done. The results of these simulations will be compared with theory.

Introduction and Summary

Fusion energy is considered as one of the most promising potential sources of virtually unlimited energy for mankind. In Magnetic Confinement Fusion (MCF), the plasma is confined using a magnetic field with nested flux surfaces at very high temperatures. The most successful present-day magnetic device for confining plasma is called "tokamak". The next-generation tokamak "International Thermonuclear Experimental Reactor (ITER)" is expected to be the penultimate step towards fusion power production (the last step envisaged being DEMO). In such fusion devices (and wherever else the plasma comes into contact with a wall), the plasma region near the wall plays an important role in determining the flow of particles and energy to the wall and the release of impurities from the latter. A proper understanding of the sheath phenomena is also an important prerequisite for obtaining boundary conditions for fluid codes simulating tokamaks.

Let us now we briefly explain how a sheath is formed at the boundary of a plasma. Suppose that when ions and electrons hit the wall they deliver their charge there. Since electrons have much higher thermal velocities than ions, the wall is charged up negatively with respect to the surrounding plasma (Fig.1). The negative potential then attracts the ions and repels part of the electrons, forming a positive-space-charge region in front of the wall. This positive-space-charge region, known as the "sheath" (also called "electrostatic" or "Debye" sheath), separates the negatively charged wall from the quasineutral "presheath" plasma. The case with zero net electric current flow, i.e., of equal electron and ion fluxes to the wall, is usually referred to as the "floating" case, and the related wall potential is called the "floating potential". For the floating case the height of the barrier adjusts itself so that the flux of electrons that have enough energy to go over the barrier to the wall is just equal to the flux of ions reaching the wall. The potential falls off rapidly as we move towards the wall, so that the electric field is relatively strong and the motion of the plasma is dominated by the electric (rather than magnetic) forces.

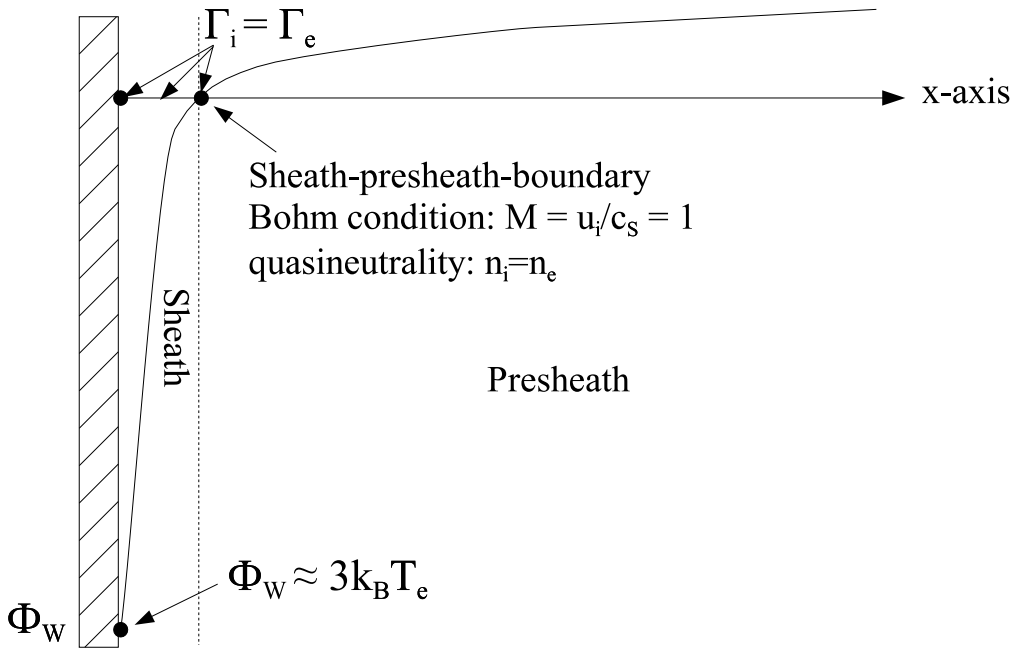

Figure 1: General structure of the PWT region without magnetic field.

When high-energy particles (more than 5-10eV) are hitting the wall, secondary electrons can be ejected. These secondary electrons are accelerated in the sheath potential, so that at the sheath entrance they represent a pronounced beam propagating into the presheath. If the corresponding electron-beam instability is stronger than the damping processes in the presheath, the presheath becomes unstable. In this thesis we treat the influence of the secondary electrons using both theory ([18]) and particle-in-cell (PIC) simulations.

Particle simulations are especially important for the simulation of the sheath, which cannot be treated by fluid codes due to the strongly nonequilibrium character of the related electron and ion distributions. The model underlying a PIC algorithm consists of charged particles moving under the influence of forces due of their own and applied fields. The fields are calculated from Maxwell's equations by knowing the positions and velocities of all particles; the forces on the particles are found using the ensuing electric and magnetic fields in the Newton-Lorentz equation of motion. One calculates the fields from the instantaneous macroscopic charge and current densities, then moves the particles (small time steps and distances) and recalculates the macroscopic densities and fields due to the particles at their new positions

and velocities; this procedure is repeated for many time steps. In e.g., the the PIC code BIT1 ([19]), the basic algorithm is extended to allow for collisions between particles. PIC simulations are very expensive computationally. Our final simulations included about $4 \cdot 10^5$ individual particles, which have to be treated in each time step. The number of time steps was about $2 \cdot 10^6$. As a consequence, each simulation needed several days to finish.

This thesis is organized as follows:

Chapter 1 includes those elements of plasma theory and PIC algorithms which are most important for this thesis. Section 1.1 presents a brief description of the basic equations for kinetic and fluid theory. Then a basic treatment of the plasma-wall-transition (PWT) is given. Section 1.1.4 gives arguments for using the unbounded-plasma dispersion relation in section 2. In Section 1.1.5 we look at the instability induced by a low-density beam in a cold, uniform plasma ([8]), which turns out to be a good approximation to the dispersion relation for a low-density beam of secondary electrons in the presheath. The result of this fluid analysis is that we can expect to see an instability with $\omega \approx ku$ (u is the group velocity of the secondary electrons). Section 1.2 includes the basic description of a PIC algorithm ([1]) and some remarks about BIT1 ([19]). For the reader interested in running PIC simulations himself, Section 1.2.6 contains some practical considerations about how to set input parameters such as the grid size and the length of a time step.

Chapter 2 is devoted to the theoretical treatment of the instability induced in the presheath by secondary electrons ([18]). The first two sections contain the formal description of the problem including the motivation for the choice of the boundary conditions at the sheath edge. In Sec.2.3 the 0^{th} order (time independent) solution of the system of differential equations is found. The dispersion relation is derived in Sec.2.4. The numerical solution ([4]) of the dispersion relation shows that we can expect an instability induced by the secondary electrons for $k\lambda_D$ slightly less than 1.

In Chapter 3 we present the results of the PIC simulations performed with BIT1. In Sec.3.2 we look at the influence of the secondary electrons on the basic plasma parameters such as density, potential, electric field, temperature and mean velocities. In Sec.3.3 we compare the results of the simulation with the 0^{th} order model. Finally, in Sec.3.4, we show that the instability is, in fact, seen in the simulation.

In addition to these results, which are already known in principle, we propose a mechanism which saturates the instability. As the (initially cold,

i.e., $T_{se} = 0$) secondary electron beam enters the presheath, its temperature rises. Due to this temperature rise, the minimum in the total electron velocity distribution gets so shallow that the Penrose criterion for instability is not fulfilled any more. Further investigations will include a theoretical treatment, in which the secondary electrons are no longer assumed to be a cold beam. Additional simulations will be done aiming at a detailed comparison of the results with the theory.

About notation: in kinetic integrals we will sometimes write

$$\int f(x,v)dv \quad \text{instead of} \quad \int_{-\infty}^{\infty} f(x,v)dv.$$

Velocities as arguments in kinetic distributions are called v, whereas fluid velocities are called u; v_{th} denotes the *electron* thermal velocity, the ion thermal velocity will be $v_{th,i}$. A detailed list of symbols can be found at the end of the thesis.

Chapter 1

Fundamentals

1.1 Plasma Theory

1.1.1 Equations of Kinetic Theory

In this Section we will state the most important equations of kinetic theory and give the necessary definitions.

In kinetic theory each plasma particle species α is described by a function $f_\alpha(x, v, t)$ for x, v and t being the space, velocity and time variables, respectively. For convenience we will from now on omit the superscript α, because in this work there is no danger of confusing different particle species. Generally x and v are 3-dimensional quantities $(3d, 3v)$, however we will often deal with situations where both x and v are 1-dimensional $(1d, 1v)$ or situations, where x is 1-dimensional and v is 3-dimensional $(1d, 3v)$. The function $f(x, v, t)$ has to be interpreted in the sense of a continuous probability distribution function. That means

$$\int_{\Delta^3 x, \Delta^3 v} f(x, v, t)\, d^3x\, d^3v$$

is the probability to find the particle at time t in a volume $\Delta^3 x$ with velocities in $\Delta^3 v$. Important quantities can be defined using moments M_k of f. The particle density is obtained as

$$n(x) = M_0(x) := \int_{-\infty}^{\infty} f(x, v, t)\, d^3v. \tag{1.1}$$

The particle flux density Γ can be derived from f as

$$\Gamma(x) = M_1(x) := \int_{-\infty}^{\infty} v f(x, v, t)\, d^3v,$$

and the mean velocity u is given by

$$u(x) = \Gamma(x)/n(x). \tag{1.2}$$

We will also need the effective temperature

$$\frac{3}{2} k_B T(x) = \int_{-\infty}^{\infty} m \frac{(v - u(x))^2}{2} f(x, v, t)\, d^3v.$$

Note that in the 1-dimensional case the equation for the effective temperature would have the factor $1/2$ instead of the factor $3/2$. The differential equation for f is given by

$$\frac{D}{Dt} f = \left(\frac{\partial f}{\partial t} \right)_C, \tag{1.3}$$

where $(\partial f/\partial t)_C$ is the collision term and

$$\frac{D}{Dt} = \frac{\partial}{\partial t} + v \cdot \frac{\partial}{\partial x} + a \cdot \frac{\partial}{\partial v},$$

with a the macroscopic acceleration on a particle, is called the convective derivative. The dots in the definition of the convective derivative indicate scalar products.

In addition, the Maxwell equations

$$\begin{aligned} \nabla \cdot B &= 0 \\ \nabla \cdot E &= -\frac{\rho}{\epsilon_0} = -\frac{1}{\epsilon_0} \sum_\alpha q_\alpha n_\alpha \\ \nabla \times B &= \mu_0 j + \frac{1}{c^2} \frac{\partial E}{\partial t} = \mu_0 \sum_\alpha q_\alpha u_\alpha + \frac{1}{c^2} \frac{\partial E}{\partial t} \\ \nabla \times E &= -\frac{\partial B}{\partial t} \end{aligned} \tag{1.4}$$

must be fulfilled. So the set of equations to be solved with appropriate initial and boundary conditions consists of (1.3) and (1.4), for which n and j have to be used from (1.1) and (1.2). Note that in electrostatic problems the only Maxwell equation considered is the Poisson equation

$$\Delta \Phi = \nabla \cdot E = -\frac{1}{\epsilon_0} \sum_\alpha q_\alpha n_\alpha \tag{1.5}$$

where the relation $E = -\nabla \Phi$ has been used.

1.1.2 Equations of Fluid Theory

Fluid theory is a simpler theory than kinetic theory, in the sense that it can be derived from kinetic theory [3]. In fluid theory we are basically dealing with a small number of velocity moments, such as n, u and T, rather than with the full velocity distribution. So we know at time t and at position x only the mean velocity $u(x)$, where in kinetic theory we know the whole velocity distribution function at position x. Consequently, all effects for which the detailed shape of the velocity distribution function is important (such as Landau damping), cannot be explained by fluid theory. In many situations (typically for high collisionality) fluid theory is a very good model and there is no need for using kinetic theory.

In fluid theory, the equations for $n(x)$ and $u(x)$ of ions and electrons are the continuity equation

$$\frac{\partial n}{\partial t} + \nabla \cdot (nu) = S(x,t)$$

and the momentum equation

$$\begin{aligned} mn\left(\frac{\partial u}{\partial t} + (u\cdot\nabla)u\right) &= -\nabla p + qn(E + u\times B) + mg \\ &\quad -mu\nu n_n - muS(x,t). \end{aligned}$$

We have a force coming from the pressure gradient ∇p, the Lorentz-force and the gravitational force mg. We also have a force from collisions with neutrals described by the neutral density n_n and the collision frequency ν and from ionization. These equations again have to be solved together with the Maxwell equations (1.4) and (usually) the equation of state

$$p = nk_BT. \tag{1.6}$$

Generally one also needs an equation for T, however in this thesis we "close the hierarchy" by setting the temperature to a given value.

For the electrons in steady state (in electrostatic situations or in the direction along B) often the following approximation is made: one considers the equation

$$0 = -\nabla p_e - enE,$$

which leads together with (1.6) to the Boltzmann distribution

$$n_e(x) = n_0 e^{e\phi(x)/k_BT_e}. \tag{1.7}$$

1.1.3 Plasma-Wall-Transition (PWT)

Suppose there is no appreciable electric field inside the plasma; we can then let the potential ϕ be constant there. Suppose that when ions and electrons hit the wall they deliver their charges there. Since electrons have much higher thermal velocities than ions, they are lost faster and leave the plasma with a net positive charge. Hence, the wall must have a potential negative with respect to the plasma. This potential cannot be distributed over the entire plasma because Debye shielding will confine the potential variation to a layer of the order of several Debye lengths in thickness. This layer is called a sheath. The function of a sheath is to form a potential barrier, so that the electrons are confined electrostatically. The height of the barrier adjusts itself so that the flux of electrons that have enough energy to go over the barrier to the wall is just equal to the flux of ions reaching the wall. Note that the sheath potential, while reflecting or at least slowing down the electrons, accelerates the ions towards the wall.

1.1.3.1 Bohm Criterion

We now derive the Bohm criterion, starting with the derivation of the so-called non-marginal Bohm criterion which comes from the consideration of the sheath scale in the usual two-scale analysis [13].

We consider the fluid equations in one dimension for the time-independent, electrostatic case with cold ions. We consider the floating case, where the potential is monotonically decreasing towards the wall. We assume that the sheath is so thin that collisions and ionization sources can be neglected. The sheath is also assumed to be so thin that the wall can be regarded as plane. In terms of the two-scale analysis this is the case $\epsilon := \lambda_D/L \to 0$ for L the relevant collision length. Later we will see that the length of the sheath is about 10 Debye lengths, which is much smaller than the mean free path in our case, so this assumption is reasonable. At the sheath edge the plasma is quasineutral. For the electrons we assume the Boltzmann distribution, in the region of the sheath edge this is a very good approximation. We set the axis such that the sheath edge is at $x = 0$. We also choose the potential to be zero at the sheath edge, so when n_0 denotes the electron density at the sheath edge, the Boltzmann distribution can be written as

$$n_e(x) = n_0 e^{e\phi(x)/k_B T_e}. \tag{1.8}$$

Since we are interested in the steady state ($\partial/\partial t = 0$) the ion continuity

equation results in

$$\frac{d}{dx}(n_i u_i) = 0. \tag{1.9}$$

For the ions we additionally need the momentum equation

$$m_i u_i \frac{du_i}{dx} = eE = -e\frac{d\phi}{dx}. \tag{1.10}$$

Since we are dealing with the electrostatic case, we use the Poisson equation

$$\frac{d^2\phi}{dx^2} = \frac{e}{\epsilon_0}(n_e - n_i). \tag{1.11}$$

Since we consider the floating case, the flux of electrons and ions to the wall must be the same, so

$$\Gamma_e = \Gamma_i, \quad \text{i.e. } n_e u_e = n_i u_i. \tag{1.12}$$

We can omit the electron continuity equation

$$\frac{d}{dx}(n_e u_e) = 0.$$

because it follows from the flux equality and the ion continuity equations.

Having stated the model we start with the Poisson equation (1.11). We insert the electron density from the Boltzmann relation (1.8) and the ion density from the continuity equation (1.9) using the quasineutrality at the sheath edge

$$\frac{d}{dx}(n_i u_i) = 0 \Rightarrow n_i u_i = n_{i,0} u_{i,0} = n_0 u_{i,0} \Rightarrow n_i = \frac{n_0 u_{i,0}}{u_i}.$$

Hence, the Poisson equation becomes

$$\frac{d^2\phi}{dx^2} = \frac{n_0 e}{\epsilon_0}\left(e^{e\phi(x)/k_B T_e} - \frac{u_{i,0}}{u_i}\right). \tag{1.13}$$

To express u_i in terms of the potential we use the ion momentum equation (1.10) in the form

$$m_i u_i \frac{du_i}{dx} = \frac{1}{2} m_i \frac{du_i^2}{dx} = -e\frac{d\phi}{dx}.$$

Integration over x leads to

$$u_i = \sqrt{-\frac{2e}{m_i}(\phi + C)}$$

where C is the integration constant, which we determine using our convention that for $x = 0$ we have $\phi = 0$ and $u_i = u_{i,0}$. Hence we obtain

$$u_i = u_{i,0}\sqrt{1 - \frac{2e\phi}{m_i u_{i,0}^2}} = u_{i,0}\sqrt{1 - 2\frac{e\phi}{k_B T_e}\frac{1}{M_0^2}}, \quad \text{with } M_0 := \frac{u_{i,0}}{c_S},\ c_S = \sqrt{\frac{k_B T_e}{m_i}}$$

which we substitute in (1.13) to get

$$\frac{d^2\phi}{dx^2} = \frac{n_0 e}{\epsilon_0}\left(e^{e\phi(x)/k_B T_e} - \left(1 - 2\frac{e\phi}{k_B T_e}\frac{1}{M_0^2}\right)\right).$$

Now we consider the region near the sheath edge. Since at the sheath edge we have $\phi = 0$, we can expand the right-hand side up to first order in $e\phi/k_B T_e$, leading to

$$\frac{d^2\phi}{dx^2} = \frac{n_0 e^2 \phi}{\epsilon_0 k_B T_e}(1 - \frac{1}{M_0^2}). \tag{1.14}$$

We are searching for a potential ϕ which is monotonically decreasing towards the wall. This just means that in the region from the sheath edge to the wall we must have

$$\frac{d^2\phi}{dx^2} \leq 0 \quad \text{for } \phi \leq 0.$$

From (1.14) we see that this condition can only be fulfilled if

$$M_0 \geq 1 \tag{1.15}$$

This condition for the ion velocity at the sheath edge is called the (non-marginal) Bohm criterion. It is often written in the form

$$u_{i,0} \geq c_S = \sqrt{\frac{k_B T_e}{m_i}}.$$

However, the Bohm criterion is fulfilled usually in its marginal (equality) form. Let us now look at the presheath scale to get the marginal form of the Bohm criterion. In the presheath scale ($L \gg \lambda_D$) collisions (ν_i), sources (S_i) and the geometry (A, e.g. $A(x) = 4\pi(R \pm x)^2$) must not be neglected. The equations we consider [13] are the ion continuity equation

$$\frac{d}{dx}(n_i u_i) = S_i - \frac{A'}{A} n_i u_i \tag{1.16}$$

and the ion momentum equation

$$m_i u_i \frac{du_i}{dx} + e\frac{d\phi}{dx} + \frac{\gamma_i k_B T_i}{n_i} = -\left(\nu_i + \frac{S_i}{n_i}\right) m_i u_i. \tag{1.17}$$

Expressing the term du_i/dx using (1.16) and $d\phi/dx$ using the definition of T_e^* and the quasineutrality condition we get

$$\left[m_i u_i^2 - k_B(T_e^* + \gamma_i T_i)\right] \frac{dn}{dx} = m_i u_i (n\nu_i + 2S_i - n\frac{A'}{A}) \tag{1.18}$$

We have a singularity $dn/dx = \pm\infty$ (and therefore, using the Boltzmann relation, $d\phi/dx = \pm\infty$) if the bracket $[\ldots]$ on the left hand side vanishes (since we consider plane walls $A' = 0$ the right side is positive), i.e. if the Bohm criterion is fulfilled with the equality sign

$$M_0 = 1. \tag{1.19}$$

The singularity indicates the breakdown of the quasi-neutral approximation and represents the sheath edge. So we have the important result that the Bohm criterion is fulfilled usually in its marginal (equality) form.

Note that this definition of the ion sound velocity is consistent with the more general definition [13]

$$c_S = \sqrt{\frac{\gamma_i k_B T_i + k_B T_e^*}{m_i}}, \tag{1.20}$$

with

$$\frac{k_B T_e^*}{e} = n_e \frac{d\phi}{dn_e}\bigg|_{se} \text{ and } \gamma_i = 1 + \frac{n_i}{dn_i/d\phi}\frac{dT_i/d\phi}{T_i}\bigg|_{se} \tag{1.21}$$

because we assumed cold ions and $T_e^* = T_e$ holds for the Boltzmann relation.

1.1.3.2 Potential Drop and Thickness of the Sheath

Now we use the Poisson equation (1.11) for a simple estimation of the characteristic scale length of the sheath. For this purpose we make a scale analysis of (1.11)

$$\frac{\phi}{\phi_{\text{ref}}}\frac{1}{L_S^2} \sim \frac{e n_{\text{ref}}}{\epsilon_0 \phi_{\text{ref}}}\left(\frac{n_e}{n_{\text{ref}}} - \frac{n_i}{n_{\text{ref}}}\right),$$

where L_S denotes the characteristic length. Setting $\phi_{\text{ref}} \sim k_B T_e/e$ and $n_{\text{ref}} = n_0$ we find

$$L_S \sim \sqrt{\frac{n_0 e^2}{\epsilon_0 k_B T_e}} = \lambda_D.$$

Note that in practice the length of the sheath is about a few λ_D.

According to the Bohm criterion the ions arrive at the sheath edge with the ion sound velocity. Usually this is explained by a potential drop in the so-called presheath, where the ions get accelerated. The corresponding potential

drop $\Delta\phi_{PS}$ is

$$\frac{1}{2}m_i c_S^2 \simeq |e\Delta\phi_{PS}| \Rightarrow |e\Delta\phi_{PS}| \approx \frac{1}{2}k_B T_e. \tag{1.22}$$

For practical considerations (see Sec.1.1.3.3) the potential drop across the sheath, $\Delta\phi_S$, and the ion and electron fluxes to the wall, $\Gamma_{e,wall}$ and $\Gamma_{i,wall}$, are important as well. The potential drop can be derived from the equality of the electron and ion fluxes, which is intuitively plausible because during the formation of the sheath the wall potential just adjusts its height in order to balance the ion and electron fluxes to the wall. For the ions we get the flux directly from the conservation of particle flux (1.9) and the marginal Bohm criterion (1.19)

$$\Gamma_{i,wall} = \Gamma_{i,0} = n_0 c_S. \tag{1.23}$$

We can in addition relate the density in the Boltzmann relation at the sheath edge, n_0, to the density of the bulk plasma, n, considering the potential drop across the presheath. Note that the presheath is quasineutral, so the Boltzmann relation holds not only for the electron but also for the ion density there.

$$n_0 = e^{-|e\Delta\phi_{PS}|}n \approx 0.6n \tag{1.24}$$

Combining (1.23) and (1.24) leads to

$$\Gamma_{i,wall} = 0.6nc_S \tag{1.25}$$

For the electrons we can treat the flux as a flux of a Maxwellian to a wall. Using

$$\Gamma_{e,wall} := \int_0^\infty \int_{-\infty}^\infty \int_{-\infty}^\infty v_x f^{\mathrm{Max}}(v)\, dv_x\, dv_y\, dv_z = \frac{1}{4}n_{e,wall}u_{e,wall},$$

with

$$u_{e,wall} := \int_{-\infty}^\infty |v| f^{\mathrm{Max}}(v)\, d^3v = \sqrt{\frac{8k_B T_e}{\pi m_e}}$$

and

$$f^{\mathrm{Max}}(v) := \left(\frac{m}{2\pi k_B T}\right)^{3/2} \exp\left(-\frac{mv^2}{2k_B T}\right)$$

we obtain

$$\Gamma_{e,wall} = \frac{1}{4}n_0 e^{-e\Delta\phi_S/k_B T_e}u_{e,wall} = 0.6ne^{-e\Delta\phi_S/k_B T_e}\sqrt{\frac{k_B T_e}{2\pi m_e}}. \tag{1.26}$$

Equalling the electron and ion fluxes equal leads to

$$e\Delta\phi_S = -0.5 \ln \left(2\pi \frac{m_e}{m_i} \right) k_B T_e.$$

If the ions have a finite temperature as well one can use the more general expression for c_S and obtain

$$e\Delta\phi_S = -0.5 \ln \left(2\pi \frac{m_e}{m_i} \left(1 + \gamma \frac{T_i}{T_e} \right) \right) k_B T_e.$$

For equal ion and electron temperatures and hydrogenic plasmas this yields about

$$|e\Delta\phi_S| = 3 k_B T_e. \tag{1.27}$$

1.1.3.3 Consequences of the Existence of a Sheath for Tokamaks

Now we can specify some important consequences of the existence of a sheath for tokamaks ([15]).

(i) Sputtering due to ion impact on the wall is linearly dependent on Γ_i and strongly depends on the impact energy. Without a sheath the ion flux would be the flux of a Maxwellian $n\langle|v_i|\rangle/4$, with a sheath it is $n_0 c_S$. This difference is not very significant. However the ion impact energy of a Maxwellian is $2k_B T_i$, while with a sheath it is about $2k_B T_i + |e\Delta\phi_S| \approx 5 k_B T_i$.

(ii) The energy flux to the surface with a sheath is smaller than without a sheath. Without sheath the electron and ion energy fluxes to the wall q_e and q_i are given by

$$\begin{aligned} q_{i,wall} &= 2k_B T_i \frac{1}{4} n \langle|v_i|\rangle = 2 k_B T_i n \sqrt{\frac{k_B T_i}{2\pi m_i}} \\ q_{e,wall} &= 2k_B T_e \frac{1}{4} n \langle|v_e|\rangle = 2 k_B T_e n \sqrt{\frac{k_B T_e}{2\pi m_e}} \end{aligned}$$

With a sheath the ions gain an energy of $|e\Delta\phi_S|$ in the sheath. So, using (1.25) and (1.27), the ion energy flux to the wall becomes

$$q_{i,wall} = (2k_B T_i + |e\Delta\phi_S|)\Gamma_i = (2k_B T_i + 3k_B T_e) 0.6 n c_S.$$

The electron heat flux to the wall is, using (1.26) and (1.27),

$$q_{e,wall} = 2k_B T_e \Gamma_e = \exp(-3) 2 k_B T_e 0.6 n \sqrt{\frac{k_B T_e}{2\pi m_e}}.$$

In summary the sheath increases the ion heat flux to the wall by a factor of two, while decreasing the electron heat flux to the wall by a factor of 20, giving an overall reduction by about an order of magnitude. The sheath serves to protect the solid surface from plasma heat.

(iii) For a plasma such as the tokamak edge, the input power is given. Looking at (ii) it is clear that, for a given input power and total plasma energy content, the resulting edge n and T will be quite different with and without a sheath. So it is essential to include the sheath properties as boundary conditions in modelling the edge plasma.

1.1.4 Stability of the Pierce diode for big systems

In section 2 we investigate the stability properties of the presheath using a dispersion relation derived for an unbounded plasma. This approach is thought to be justified if the system is large. To examine this justification further we consider the dimensionless eigenfrequency equation of the short-circuited Pierce diode [6, 7] as a model system:

$$D_{Pierce}(\eta) = e^{i\alpha\eta}[(\eta^2+1)\sin\alpha + 2i\eta\cos\alpha] + \alpha\eta^4 - \alpha\eta^2 - 2i\eta = 0. \quad (1.28)$$

Here $\eta := \omega/\omega_p$ is the normalized frequency and $\alpha := Lu_0/\omega_p$ is the normalized length of the system. We want to show that for "long" systems ($\alpha \to \infty$) the growth rates of the most unstable solutions converge to zero.

The solutions of this eigenfrequency equation depend on the normalized length α. In principle the method of choice is to find all analytic solutions $\eta(\alpha)$ and to then perform the limit $\alpha \to \infty$. However, this is not feasible analytically because the eigenfrequency equation is a sum of an exponential term and a polynomial in α. Hence we have solved (1.28) numerically using values from the numerical solutions given in [11] as starting values. The results of [11] were confirmed (Figs. 1.1 and 1.2). One can identify two different sets of solutions. The first set $\eta^m(\alpha)$ is characterized by the property that the starting point of the curve is at $2m\pi,\ m \in \mathbb{N}$ (Fig.1.1). The real part of these solutions starts at zero, increases with α and tends to 1 for $\alpha \to \infty$. The imaginary part also starts at zero, increases with α, reaches its maximum at $\alpha = 2m\pi + \pi/2$, decreases and gets negative. These solutions are oscillatory; they are unstable (exponentially) for $\mathrm{Im}(\eta^m) > 0$ and stable (exponentially decaying) for $\mathrm{Im}(\eta^m) < 0$.

The second set of solutions $\eta^l(\alpha)$ is characterized by the property that the starting point of the curve is at $(2l+1)\pi,\ l \in \mathbb{N}_0$ (Fig.1.1). The real part

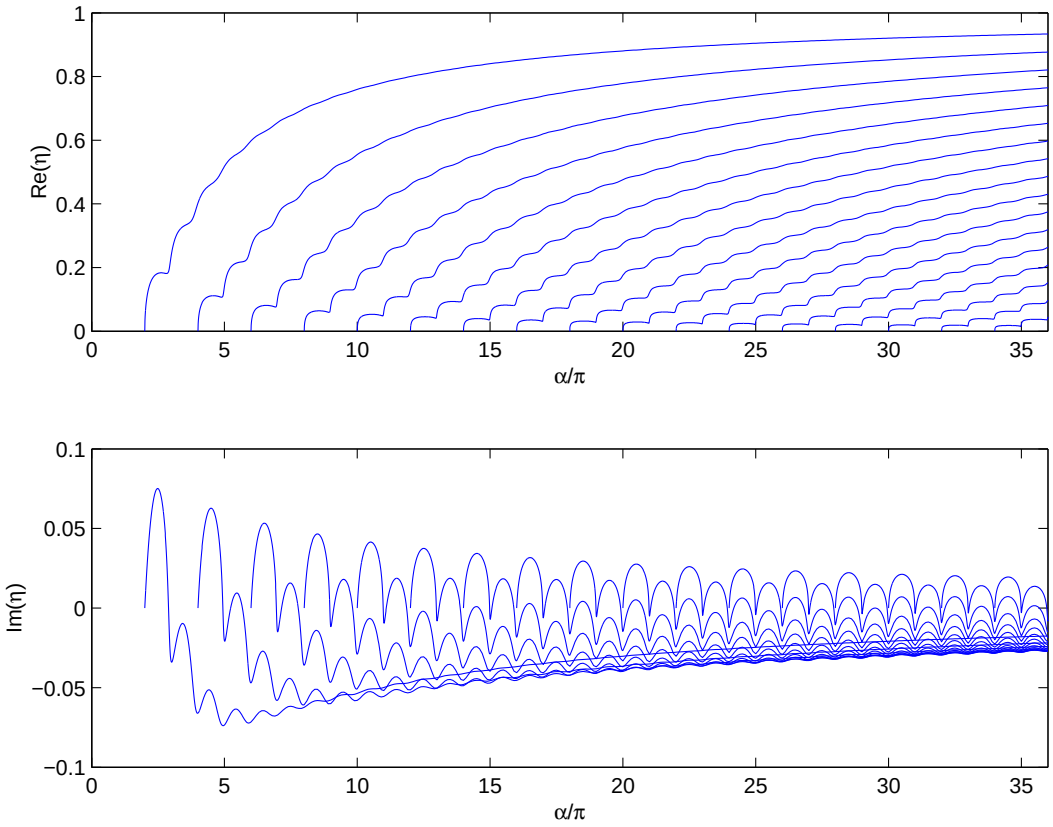

Figure 1.1: Oscillatory solutions $\eta^m(\alpha)$ of (1.28), having the property $\mathrm{Re}(\eta^m(\alpha)) \neq 0$.

of these solutions stays zero. The imaginary part starts at zero, increases with α, reaches its maximum at $\alpha = (2l+1)\pi + \pi/2$, decreases and becomes strongly negative. These solutions are non-oscillatory. They are exponentially growing for $\mathrm{Im}(\eta^l) > 0$ and exponentially decaying for $\mathrm{Im}(\eta^l) < 0$.

Since we are here interested in long systems, we additionally investigated the behavior of the solutions up to $\alpha/\pi = 1000$ instead of just $\alpha/\pi = 36$ (as was done in [11]). The dominant mode of the oscillatory solutions in the range $\alpha \in [2m\pi, 2m\pi + 2\pi]$ is just the solution $\eta^m(\alpha)$. To get the rate of decay of the growth rate of the dominant modes we made a fit through the maxima of the imaginary parts in this interval, i.e. through the points $\{(2m\pi + \pi/2, \mathrm{Im}(\eta^m(2m\pi + \pi/2))),\ m = 1, \ldots, 499\}$. We got very good agreement between the maxima obtained and a fit with the curve $\mathrm{Im}(\eta_{max,m}(\alpha)) = 1.73\alpha^{-0.794}$ (Fig.1.3).

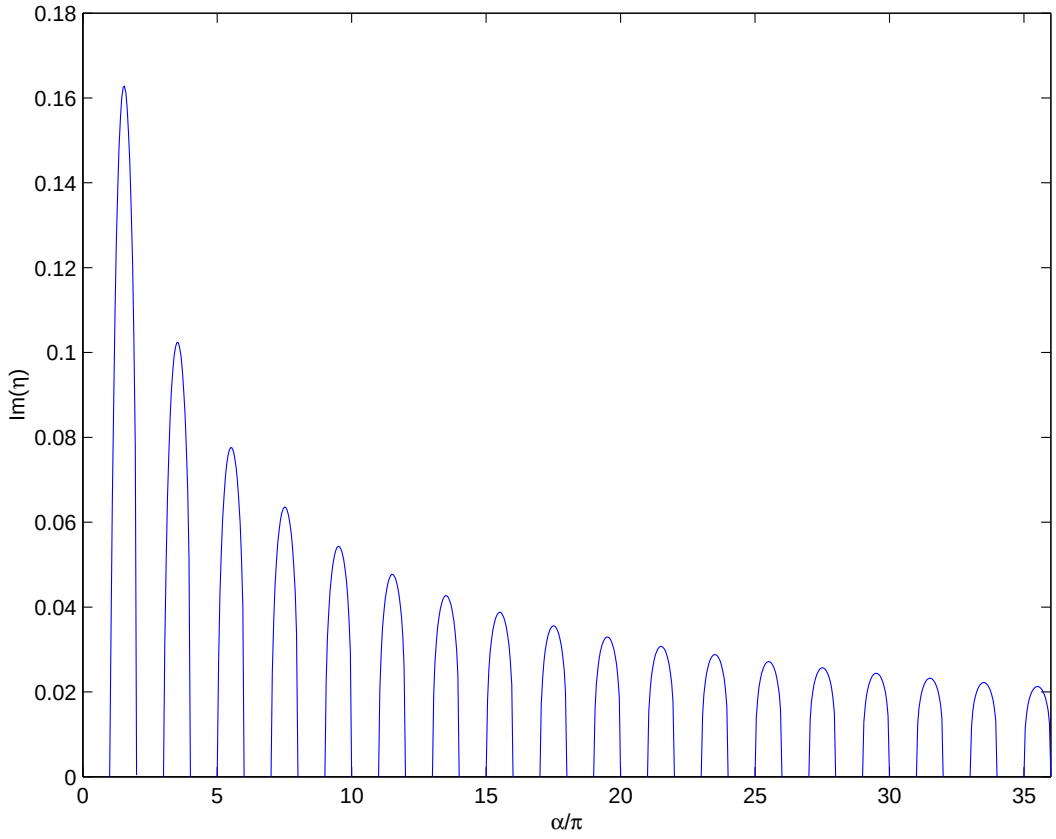

Figure 1.2: Purely growing solutions $\eta^l(\alpha)$ of (1.28), having the property $\mathrm{Re}(\eta^l(\alpha)) = 0$.

The analogous procedure for the curves $\eta^l(\alpha)$, i.e., for the non-oscillatory modes with $\alpha = (2l+1)\pi + \pi/2$ also leads to excellent agreement with the curve $\mathrm{Im}(\eta_{max,l}(\alpha)) = 1.15\alpha^{-0.827}$ (Fig.1.4).

One can estimate the rate of decay of the growth rates using the dispersion relation (1.28). We will show this estimation for the set of non-oscillatory solutions $\eta^l(\alpha)$, the set of oscillatory solutions $\eta^m(\alpha)$ can be treated analogously. Inserting $\eta = i\eta_i$ and $\alpha = (2l+1)\pi+\pi/2$ in (1.28) and approximating $1+\eta_i^2$ by 1 (we consider growth rates much smaller than 1) leads to

$$-\exp(-\alpha\eta_i) + \alpha\eta_i^2 + 2\eta_i = 0.$$

Inserting the ansatz $\eta_i(\alpha) = c\alpha^{-d}$ leads to

$$-\exp(-c\alpha^{1-d}) + c\alpha^{1-2d} + 2c\alpha^{-d} = 0. \tag{1.29}$$

We restrict our analysis to the case $c > 0$ and consider the limit $\alpha \to \infty$. For $d > 1$ the first term becomes constant and the last two terms go to zero, so

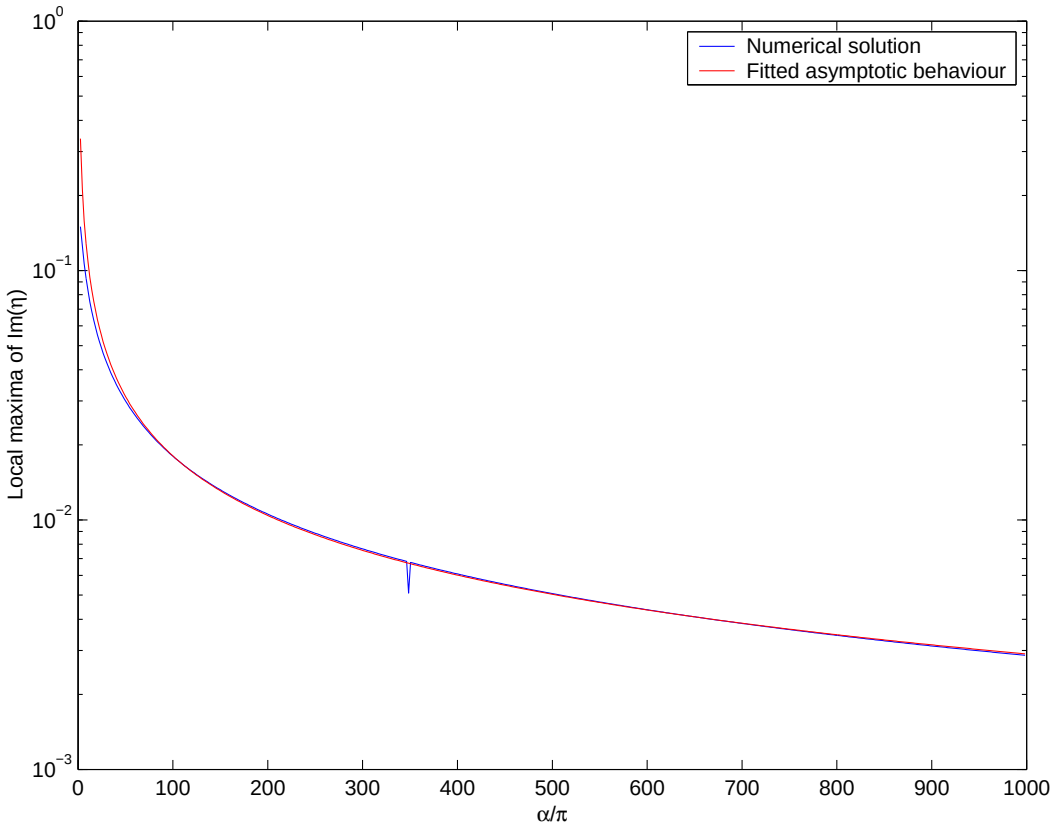

Figure 1.3: Fit through the local maxima of the imaginary part of the set of curves $\eta^m(\alpha)$, i.e., for the oscillary modes.

equation (1.29) can not be fulfilled. For $d < 1/2$ the first term goes to zero and the second term goes to infinity, so equation (1.29) can not be fulfilled. Thus we have restricted the coefficient d to the range

$$d \in [1/2\ ,\ 1]\,.$$

A comparison with the coefficients of the fits given above ($d = 0.827$ for the oscillatory solution and $d = 0.794$ for the non-oscillatory solution) shows, that indeed d is in the required range.

Summarizing this section we can say that the eigenfrequency equation of the Pierce diode has unstable solutions for each α. However, if we increase the length of the system the growth rates of the most unstable solutions decay to zero. So at least for the special case of the Pierce Diode we showed that for big enough systems the influence of the boundary on the stability properties of the plasma can be neglected. This is an argument for using the dispersion relation of the unbounded plasma in section 2.

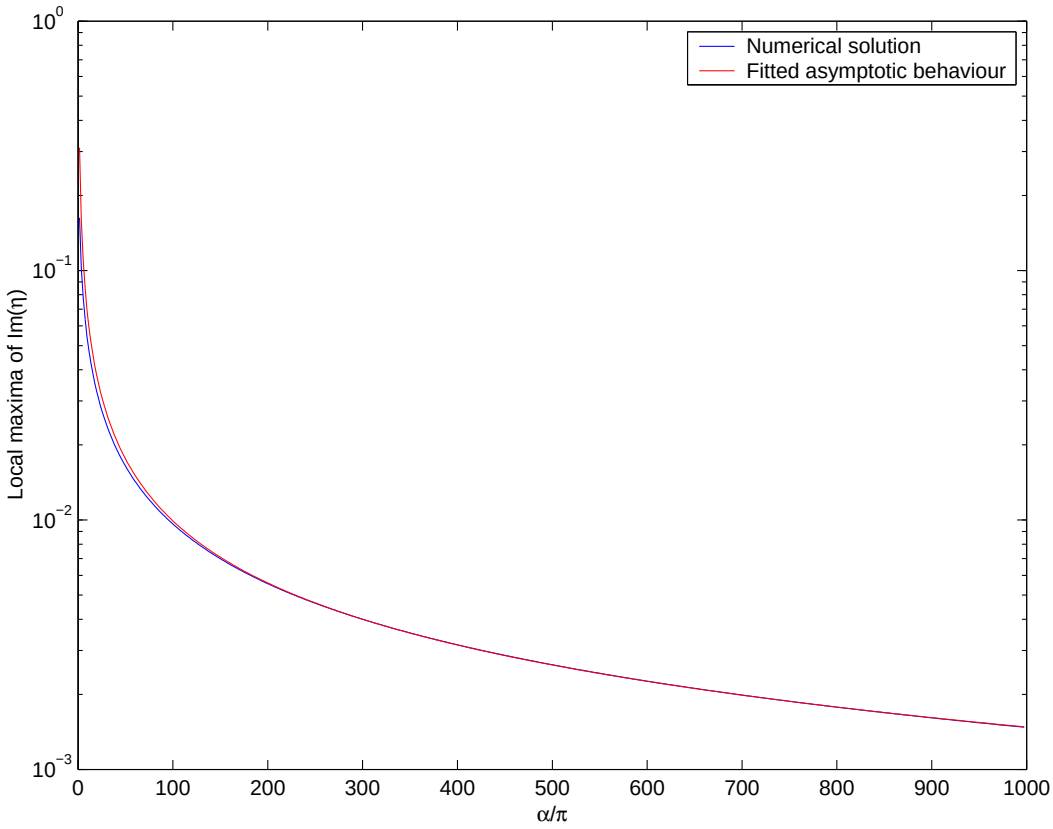

Figure 1.4: Fit through the local maxima of the set of curves $\eta^l(\alpha)$.

1.1.5 Instability of a Low-Density Beam passing through the plasma

In this section we look at instabilities of a cold, uniform, collisionless, infinite plasma [8]. We neglect any boundary conditions because we assume that the system is long enough (Sec.1.1.4). We ignore not only the thermal particle motion but also plasma nonuniformity, collisions between particles and any magnetic field. We start with the more general situation where the plasma is assumed to consist of several directed monoenergetic particle beams moving relative to each other so that the electron (or ion) distribution has the form

$$f(x,v) = \sum_{\alpha} n^{\alpha}\delta(v-u^{\alpha}),$$

where α designates the beam and n^{α} and u^{α} are the density and velocity of the particles of beam α, respectively. We restrict ourselves to electrostatic

perturbations and get (with $E = -\nabla\phi$) the following set of basic equations

$$\begin{aligned} \frac{\partial n^\alpha}{\partial t} + \nabla \cdot (n^\alpha u^\alpha) &= 0 \\ \frac{\partial u^\alpha}{\partial t} + (u^\alpha \cdot \nabla) u^\alpha &= \frac{e}{m_\alpha} E \\ \frac{\partial^2}{\partial x^2}\phi &= \frac{e}{\epsilon_0} \sum_\alpha n^\alpha. \end{aligned}$$

In this case the dispersion relation can be written ([8]) as

$$1 + \sum_\alpha \epsilon_0^\alpha = 0, \quad \text{with } \epsilon_0^\alpha = -\frac{(\omega_p^\alpha)^2}{(\omega - k u_0^\alpha)^2}. \tag{1.30}$$

It is obtained assuming small perturbations of the form

$$X^\alpha = X_0^\alpha + X'^\alpha(k, \omega) \exp(i(kx - \omega t))$$

which leads to the linearized basic equations (omitting for convenience the superscript α)

$$\begin{aligned} -i\omega n' + \nabla \cdot (n' u_0 + n_0 u') &= 0 \\ -i\omega u' + (u_0 \cdot \nabla) u' + (u' \cdot \nabla) u_0 &= \frac{e}{m} E' \end{aligned}$$

Using the continuity and momentum equation and also the uniformity assumptions

$$\nabla n_0 = 0 \text{ and } \nabla u_0 = 0$$

we obtain the perturbation of the density n' as a function of the potential. Substituting this function in Poisson's equation

$$k^2 \phi = \frac{e}{\epsilon_0} \sum_\alpha n^\alpha$$

and assuming quasineutrality

$$\sum_\alpha e n_0^\alpha = 0$$

we obtain the dispersion relation (1.30).

Now we consider a plasma consisting of electrons and ions at rest and additionally one low-density electron beam. We assume that the density of the electron beam $n^{e,\text{beam}}$ is low compared with the density n of the primary electrons , i.e., the electrons at rest

$$n^{e,\text{beam}} \ll n.$$

We shall show that a system of this kind is unstable. Regarding the ions as a neutralizing background (thus the ion term is neglected) and omitting the subscript in quantities X_0 from now on) dispersion relation (1.30) becomes ([8])

$$1 - \frac{\omega_p^2}{\omega^2} - \frac{\alpha\omega_p^2}{(\omega - k_\parallel u)^2} = 0. \tag{1.31}$$

Here we have $\alpha := n^{e,\text{beam}}/n \ll 1$ and u is the velocity of the low density electron beam.

Note that this situation is a good approximation for the dispersion relation for a low-density beam of secondary electrons in the presheath. Now we derive solutions with real part $k_\parallel u$ and group velocity $u_{gr} = u$, where u is the velocity of the secondary electrons. We will also provide growth rates of these solutions.

First we consider the dispersion relation (1.31) for the case $\alpha = 0$,

$$(\omega^2 - \omega_p^2)(\omega - k_\parallel u)^2 - \alpha\omega_p^2\omega^2 = 0. \tag{1.32}$$

from which we readily obtain the four solutions

$$\omega = \pm k_\parallel u \quad \text{and} \quad \omega = \pm\omega_p.$$

Hence, also for small α we expect two roots near $\pm k_\parallel u$ which we will consider in the following part. For these two roots we assume $|\omega - \omega_p| \gg |\omega - k_\parallel u|$, approximate $\omega^2 - \omega_p^2$ by $(k_\parallel u)^2 - \omega_p^2$ and obtain

$$((k_\parallel u)^2 - \omega_p^2)(\omega - k_\parallel u)^2 - \alpha\omega_p^2\omega^2 = 0.$$

So instead of a polynomial equation of fourth order for ω we get a polynomial equation of second order which can be solved. The solution is

$$\omega = \frac{k_\parallel u\left((k_\parallel u)^2 - \omega_p^2\right) \pm \sqrt{\alpha\omega_p^2(k_\parallel u)^2\left((k_\parallel u)^2 - \omega_p^2\right)}}{(k_\parallel u)^2 - \omega_p^2 - \alpha\omega_p}.$$

Now due to the smallness of α we can use the following approximation for the denominator

$$(k_\parallel u)^2 - \omega_p^2 - \alpha\omega_p \approx (k_\parallel u)^2 - \omega_p^2,$$

then we cancel down and get

$$\omega = k_\parallel u \pm \sqrt{\alpha}\frac{\omega_p}{\sqrt{1 - \left(\omega_p/k_\parallel u\right)^2}}.$$

If $|k_\parallel u| < \omega_p$ the term within the square root becomes negative and the second term of the derived expression for ω becomes complex. Choosing the positive root we find the growth rate

$$\gamma = \mathrm{Im}(\omega) = \sqrt{\alpha}\frac{\omega_p}{\sqrt{\left(\omega_p/k_\parallel u\right)^2 - 1}}.$$

The group velocity is then

$$u_{gr} = \frac{\partial \mathrm{Re}(\omega)}{\partial k_\parallel} = \frac{\partial (k_\parallel u)}{\partial k_\parallel} = u.$$

Summary (instability of a low-density beam):
Consider the dispersion relation (1.31) of a low-density beam ($\alpha := n_1/n_0 \ll 1$). *Then for* $\omega \approx k_\parallel u \neq \omega_p$ *two of the four roots of (1.31) are equal to*

$$\omega = k_\parallel u \pm \sqrt{\alpha}\frac{\omega_p}{\sqrt{1 - \left(\omega_p/k_\parallel u\right)^2}}. \tag{1.33}$$

If $k_\parallel u < \omega_p$ *one of these roots is complex, corresponding to an instability with growth rate*

$$\gamma = \mathrm{Im}(\omega) = \sqrt{\alpha}\frac{\omega_p}{\sqrt{\left(\omega_p/k_\parallel u\right)^2 - 1}} \tag{1.34}$$

and group velocity u.

1.2 PIC Algorithms

1.2.1 Introduction to PIC Algorithms

The model underlying a PIC algorithm consists of charged particles moving under the influence of forces due of their own and applied fields. The fields are calculated from Maxwell's equations by knowing the positions and velocities of all particles; the forces on the particles are found using the ensuing electric and magnetic fields in the Newton-Lorentz equation of motion. One calculates the fields from the instantaneous macroscopic charge and current densities, then moves the particles (small time steps and distances) and recalculates the macroscopic densities and fields due to the particles at their new positions and velocities; this procedure is repeated for many time steps. One can also extend the algorithm to allow for collisions between particles, a quite general scheme of a PIC algorithm is given in Fig.1.5

The fields are calculated on a spatial grid, which must be chosen fine enough to resolve a Debye length. The grid provides a smoothing effect by not resolving spatial fluctuations that are smaller than the grid size. The use of temporal and spatial grids, which are mathematical and not physical, causes concern about accuracy and may create "unphysical effects".

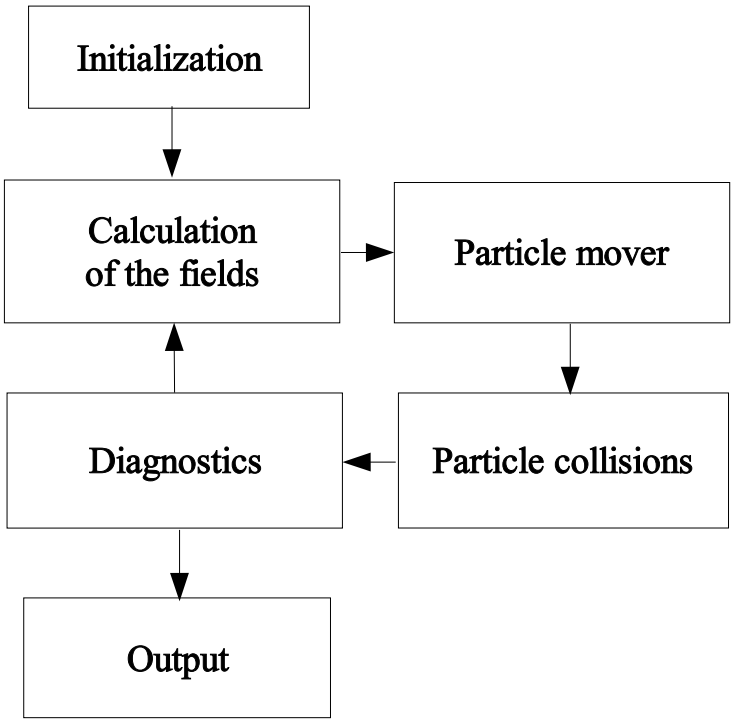

Figure 1.5: Scheme of a PIC-algorithm.

Let us now look at the algorithm in more detail. For simplicity we omit the collision and the diagnostic blocks and focus on the calculation of the electrostatic field and the particle mover. We also restrict ourselves to having a *constant* external magnetic field present. The resulting scheme is shown in Fig.1.6.

Since PIC algorithms are very time consuming, the spatial variable is most often 1-dimensional. By contrast, the velocity variable is most often 3-dimensional. An algorithm like this is said to have dimensionality (1d,3v) and is called a $(1d, 3v)$ PIC algorithm.

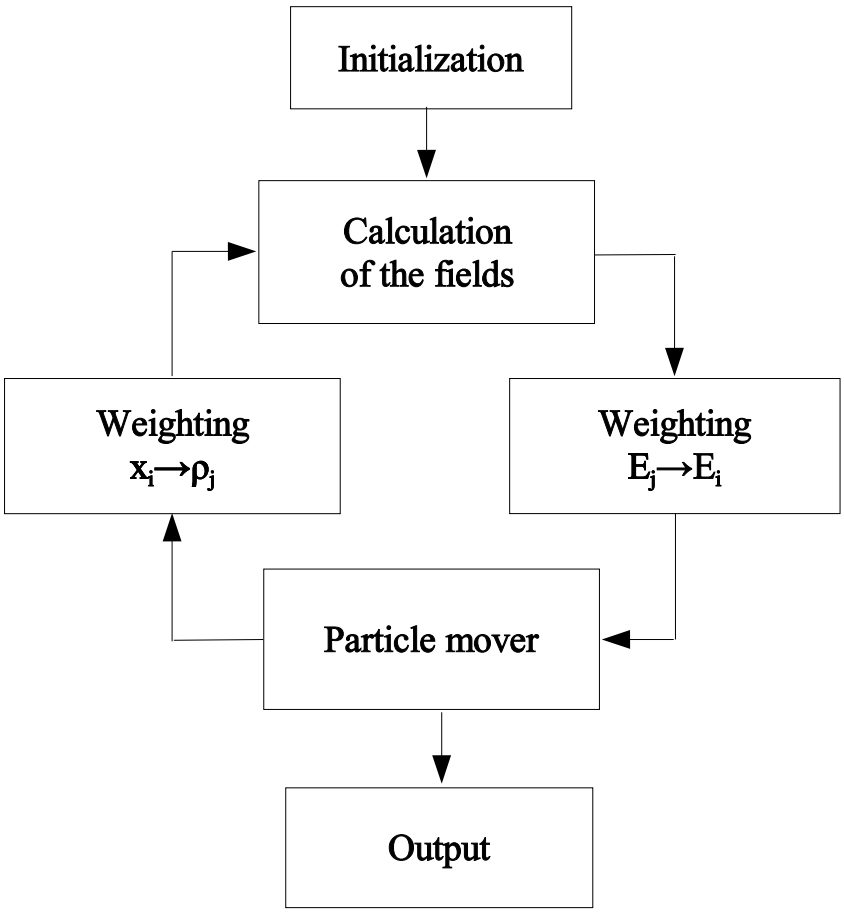

Figure 1.6: Scheme of the simplified PIC-algorithm.

1.2.2 Particle and Force Weighting

A single particle is labeled by an index i, so that its velocity and position is given by v_i and x_i. The field quantities will be obtained only on the spatial grid, consisting of discrete points in space labeled with index j its value there being E_j. The ties from the particle positions and velocities to the field quantities are made by first calculating the charge and current densities on the grid, which requires stating how to produce the grid densities from the particle velocities and positions. This process of charge and current assignment implies some weighting to the grid points that is dependent on the particle position. With the fields known on the grid but the particles scattered around in the grid, we then interpolate the fields from the grid to the particles in order to apply the force at the particle by again performing a weighting. In principle the two weighting methods can be different, however

we use the same weighting in both density and force calculations in order to avoid a self-force which would imply that a particle accelerates itself. We now describe the simplest weighting schemes.

Nearest grid point (NGP) weighting: In zero-order weighting we simply count the number of particles $N(j)$ with charge q within distance $\pm\Delta x/2$ (where Δx denotes the cell width) about the j^{th} grid point X_j and assign it to that point. The related grid density is

$$\rho_j = qN(j)/\Delta x.$$

The electric field is that at the grid position X_j for all particles in the j^{th} cell $C_j := [X_j - \Delta x/2, X_j + \Delta x/2]$

$$E(x_i) = E_j, \quad \text{for } j \in C_j.$$

As a particle moves into the j^{th} cell (through cell boundaries at $x = X_j \pm \Delta x/2$), the grid density of the j^{th} cell jumps up. This method will produce a density and an electric field which are relatively noisy both in space and time. Thus, we look out for a better weighting scheme.

Cloud in cell (CIC) weighting: The CIC model assigns a charge q_i at x_i with $X_j < x_i \leq X_{j+1}$ to its nearest grid points j and $j+1$ by linear interpolation:

$$q_j = q_i \frac{\Delta x - (x_i - X_j)}{\Delta x} = q_i \frac{|x_i - X_{j+1}|}{\Delta x}, \quad q_{j+1} = q_i \frac{|x_i - X_j|}{\Delta x}.$$

The force weighting for such a charge is done similarly:

$$E(x_i) = \frac{|x_i - X_{j+1}|}{\Delta x} E_j + \frac{|x_i - X_j|}{\Delta x} E_{j+1}.$$

Higher-order weighting by use of quadratic and cubic splines rounds off further the roughness in particle shape and reduces density and field noise, but at the cost of more computation.

More generally, choosing an interpolating function $S(x)$ called "particle shape" the weighting methods can be written as (Fig.1.7)

$$\rho_j = \sum_i q_i S(X_j - x_i)$$

and

$$F_i = q_i \Delta x \sum_j E_j S(X_j - x_i).$$

S should be designed so that the charge on the grid is the same as the total

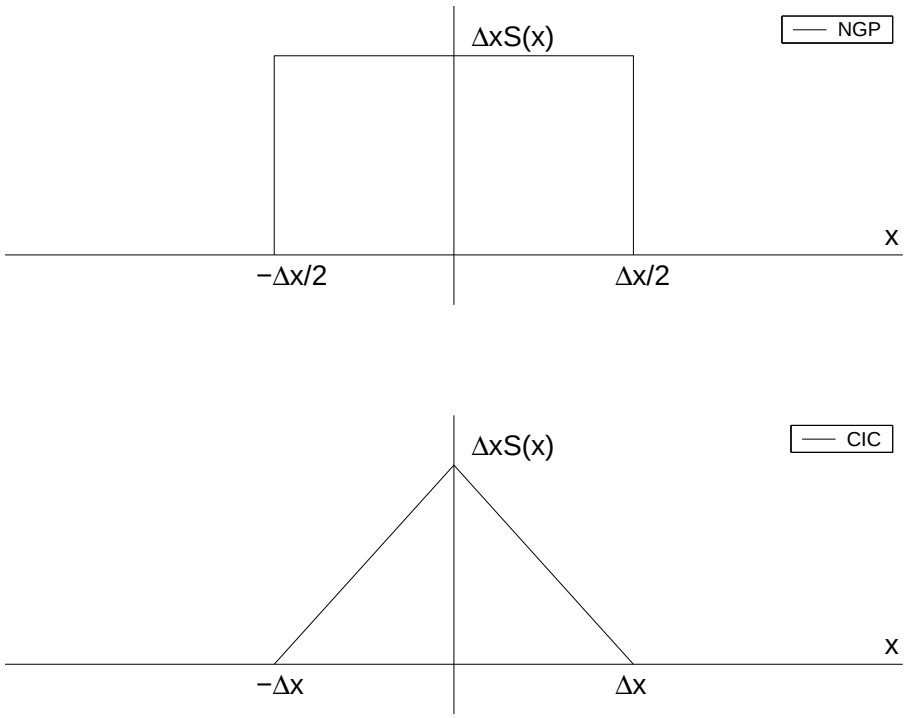

Figure 1.7: Interpolating functions for charge and force: NGP and CIC.

particle charge:

$$g\Delta x \sum_j \rho_j = \sum_i q_i.$$

For a particle at position x it follows that

$$\Delta x \sum_j S(X_j - x) = 1.$$

The statement, in CIC and higher order interpolation,

$$\Delta x \sum_j X_j S(X_j - x) = x$$

says that the charge at x makes the same, and correct contribution to dipole moments independent of the particle location ($\Delta x \sum_j \rho_j X_j = \sum_i q_i x_i$).

Additionally the algorithm should conserve the total momentum P. The change of the total momentum of the overall system dP/dt can be shown to be

$$\frac{dP}{dt} = \sum_i F_i = \Delta x \sum_j \rho_j E_j.$$

In an infinite or periodic system, if the algorithm treats all grid points in the same way and has left-right symmetry (reflection invariance), then

$$\Delta x \sum_j \rho_j E_j = 0$$

and system momentum is conserved. In the presence of boundaries $\Delta x \sum_j \rho_j E_j \neq 0$ and total momentum is not conserved.

1.2.3 Particle Mover

In this section we describe how to update the positions and velocities of the charged particles using the Newton-Lorentz equation of motion. One commonly used method is called "leap-frog" method. The two first-order differential equations to be integrated separately for each particle are

$$\begin{aligned} m\frac{dv}{dt} &= F \\ \frac{dx}{dt} &= v, \end{aligned}$$

where F is the force. These equations are replaced with the finite-difference equations

$$\begin{aligned} m\frac{v_{new} - v_{old}}{\Delta t} &= F_{old} \\ \frac{x_{new} - x_{old}}{dt} &= v_{new}. \end{aligned}$$

Note that we are using a staggered time grid. This means that x and v are not taken at the same time, but are shifted with respect to each other by $\Delta t/2$ (see also [10]). This shift is physically reasonable because we use v for the transition between two positions. However, care must be taken in the initialization step to take this time shift into account. Consider

$$F = qE + qv \times B$$

with a uniform static magnetic field $B = B_0 e_z$ along z (the $qv \times B$ force corresponds just to a rotation of v) and $E = E_x(t)e_x$ is the electric field along x (which alters the magnitude of v_x). Set

$$\omega_c = \frac{qB}{m}$$

A physically reasonable (1d,2v) scheme (with t' and t'' as dummy variables $t - \Delta t/2 < t' < t'' < t + \Delta t/2$) which is centered with respect to time is as follows:

Update of particle velocity

Half acceleration

$$\begin{pmatrix} v_x(t') \\ v_y(t') \end{pmatrix} = \begin{pmatrix} v_x(t - \frac{\Delta t}{2}) + \frac{q}{m} E_x(t) \frac{\Delta t}{2} \\ v_y(t - \frac{\Delta t}{2}) \end{pmatrix}$$

Rotation

$$\begin{pmatrix} v_x(t'') \\ v_y(t'') \end{pmatrix} = \begin{pmatrix} \cos(\omega_c \Delta t) & \sin(\omega_c \Delta t) \\ -\sin(\omega_c \Delta t) & \cos(\omega_c \Delta t) \end{pmatrix} \begin{pmatrix} v_x(t') \\ v_y(t') \end{pmatrix}$$

Half acceleration

$$\begin{pmatrix} v_x(t + \frac{\Delta t}{2}) \\ v_y(t + \frac{\Delta t}{2}) \end{pmatrix} = \begin{pmatrix} v_x(t'') + \frac{q}{m} E_x(t) \frac{\Delta t}{2} \\ v_y(t'') \end{pmatrix}$$

Update of particle position

$$x(t + \Delta t) = \left(x(t) + v(t + \frac{\Delta t}{2}) \Delta t \right).$$

1.2.4 Calculation of the electric field

Starting from the charge and current densities as assigned to the grid points, we now obtain the electric and magnetic fields, in general, from Maxwell's equations, using ρ and j as sources. Here we take this step for an electrostatic problem in one dimension x.

The differential equations to be solved are

$$\begin{aligned} E &= -\frac{\partial \phi}{\partial x} \\ \frac{\partial E}{\partial x} &= \frac{\rho}{\epsilon_0}, \end{aligned}$$

which are combined to obtain Poisson's equation

$$\frac{\partial^2 \phi}{\partial x^2} = -\frac{\rho}{\epsilon_0}.$$

One approach ([22], also used in BIT1) is to solve the finite difference equations as

$$E_j = -\frac{\phi_{j+1} - \phi_{j-1}}{2\Delta x}$$
$$\frac{\phi_{j+1} - 2\phi_j + \phi_{j-1}}{(\Delta x)^2} = -\frac{\rho_j}{\epsilon_0}$$

The main computational burden lies in solving the resulting big system of linear equations

$$A\phi = -\frac{(\Delta x)^2}{\epsilon_0}\rho,$$

where A is a large tridiagonal matrix.

1.2.5 The PIC Code BIT1

The (1d,3v) code BIT1 ([19]) was developed in Innsbruck on the basis of the XPDP1 code from the University of California at Berkeley. BIT1 has some important features: as the code from Berkeley it includes an external circuit. It has a variety of built-in collisions and includes emission of secondary electrons from the wall.

1.2.5.1 Collisions

BIT1 contains the following types of collisions:

- Coulomb collisions [16]
- Electron-neutral collisions [21]
  - Elastic scattering
  - Excitation
  - Ionization
- Ion-neutral collisions [21]
  - Elastic scattering
  - Charge exchange

In a BIT1 simulation, neutrals are not implemented as particles, but as a uniform background with density specified in the input file. The collision cross-sections can be specified in three ways: first they can be put constant, second they can have a simple shape. The third and most sophisticated option for charged-neutral collisions uses functions approximating experimental results for Hydrogen, Deuterium and Tritium [20], see Fig.1.8.

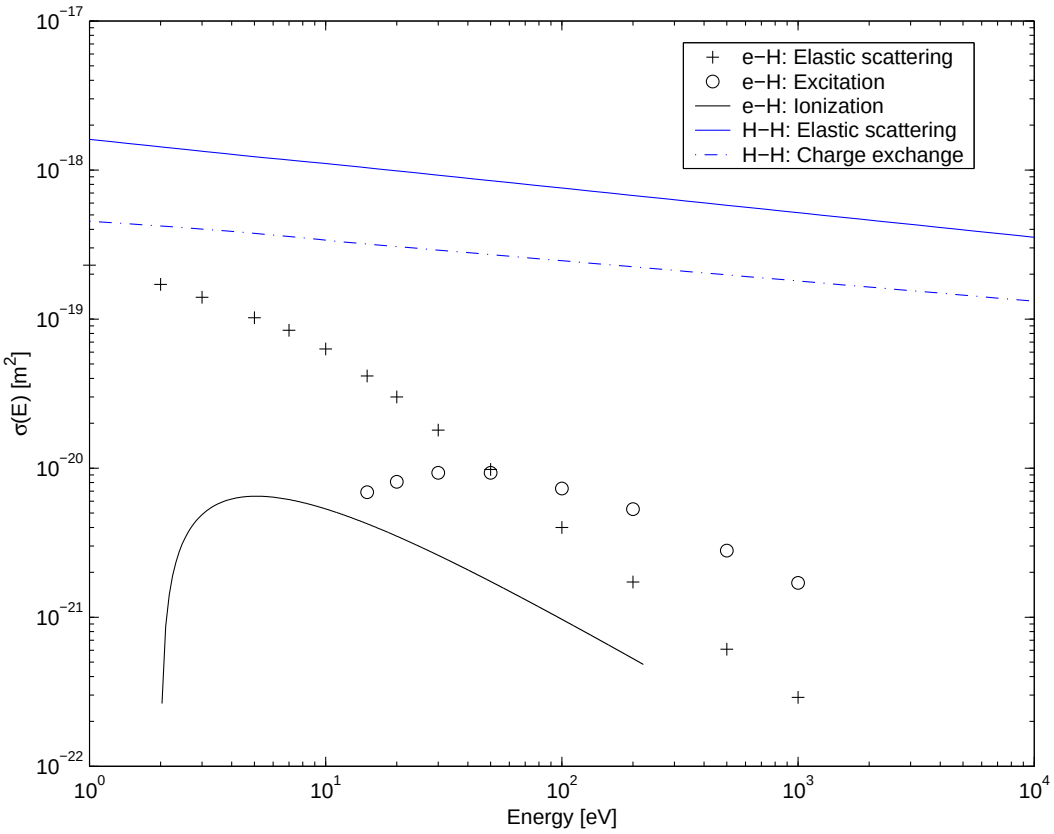

Figure 1.8: Cross sections of e-H-collisions and H-H-collisions used for BIT1.

1.2.5.2 Secondary-Electron Emission

When particles hit the wall they can induce emission of secondary electrons (SEs). BIT1 offers three different ways of including secondary electrons. The simplest method is to use a constant secondary-electron emission coefficient γ, where γ is the proportion of secondary electrons coming from the wall relative to the incoming particles.

The second method is based on experimental results for electron impact induced secondary-electron emission [17], using the formula

$$\gamma = \gamma_0 \delta(\alpha) \frac{E_p}{E_0} \exp[2 + 2\sqrt{E_p/E_0})] \quad \text{for} \quad \delta(\alpha) = \begin{cases} 1/\cos\alpha & \text{if } 1/\cos\alpha \leq 2 \\ 2 & \text{if } 1/\cos\alpha > 2 \end{cases}.$$

Here, E_p is the primary-particle energy, α is the angle of the particle incidence on the wall, and E_0 and γ_0 are constants which have to be specified in the input file.

The third method is based on experimental results for ion impact induced secondary-electron emission [12], using the formula

$$\gamma = \gamma_0 \delta(\alpha)(v_p - v_0) \quad \text{for} \quad \delta(\alpha) = \begin{cases} 1/\cos\alpha & \text{if } 1/\cos\alpha \leq 2 \\ 2 & \text{if } 1/\cos\alpha > 2 \end{cases}.$$

Here, v_p is the primary-particle velocity and v_0 and γ_0 are constants which have to be specified in the input file.

1.2.6 Practial Considerations

Running a good simulation is not trivial; a simulation program is not a black box which works fine with standard parameters. Physical knowledge is needed to correctly set parameters and to avoid unphysical effects. For example, choosing the time step Δt too big can lead to wrong frequencies of plasma oscillations (Fig.1.9). Poor simulations can even result in numerical instabilities: e.g., the so-called leapfrog algorithm for the model of a simple harmonic oscillator can lead to a nonphysical instability (Fig.1.10) if the time step Δt is chosen too large ($\Delta t > 2/\omega_0$, where ω_0 is the frequency of the harmonic oscillator).

1.2.6.1 Basic simulation conditions

To ensure that the PIC algorithm works properly, some basic conditions must be fulfilled. To achieve Debye shielding, one must have enough computer particles N_c within a Debye length λ_D, which must also be resolved by the spatial grid step. However the grid step must not be so small that a particle can pass a whole grid cell during one time step Δt. The time step must be small enough to resolve the fastest occurring oscillations ω_{max} (which is the maximum of the plasma oscillation frequency ω_p and the cyclotron frequency ω_c) [1]. Summarizing we get the following basic conditions for a proper simulation:

$$\begin{aligned} \frac{N_c}{\lambda_D} &\geq 50 \\ \Delta x &\leq \lambda_D \\ \Delta x &\geq v_{max}\Delta t \\ \Delta t &\leq \frac{0.2}{\omega_{max}} \end{aligned} \tag{1.35}$$

Often v_{max} is chosen as $3v_{th}$ or - if the heat flux has to be resolved accurately - as $5v_{th}$. Moreover one usually sets $\Delta x = \lambda_D/2$ and $N_c = 200$ and chooses

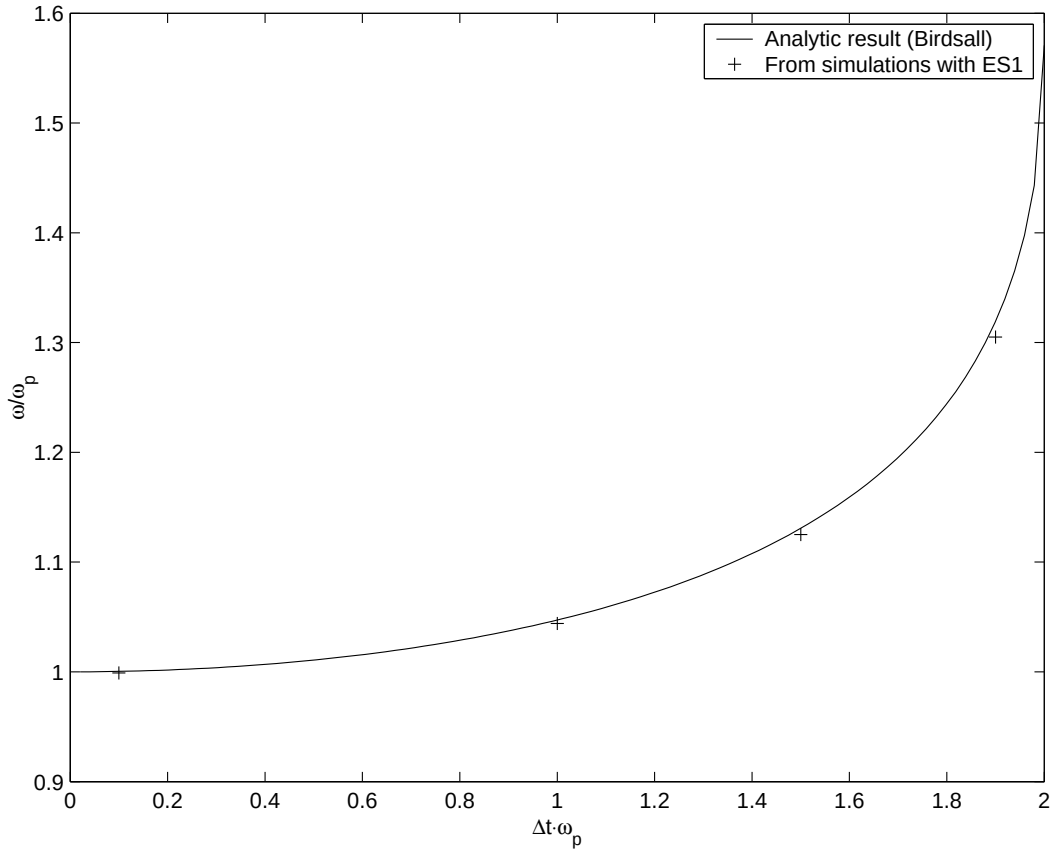

Figure 1.9: Effect of the finite time step on the frequency of plasma oscillations: ω denotes the frequency of the simulation.

Δt small enough to satisfy the last two inequalities. The larger the system the more particles are needed, which has a big influence on the simulation time. Simulations involving about 10^6 particles are feasible (depending on the machine). Note that for the calculation of λ_D and v_{th} one has to know in advance the resulting density n and electron temperature T_e.
If one only wants to simulate the sheath, the conditions (1.35) are sufficient because one only has to simulate a region consisting of about 10 Debye lengths, so that N_c does notget too large. If, however, the simulation region also includes the presheath, collisions have to be accounted for and another condition has to be fulfilled. This is because in a BIT1 simulation neutrals form an artificial background. When a neutral is ionized, a new ion is created but the neutral background does not change. This can lead to the situation that in the system more ions are produced than are lost to the wall. The

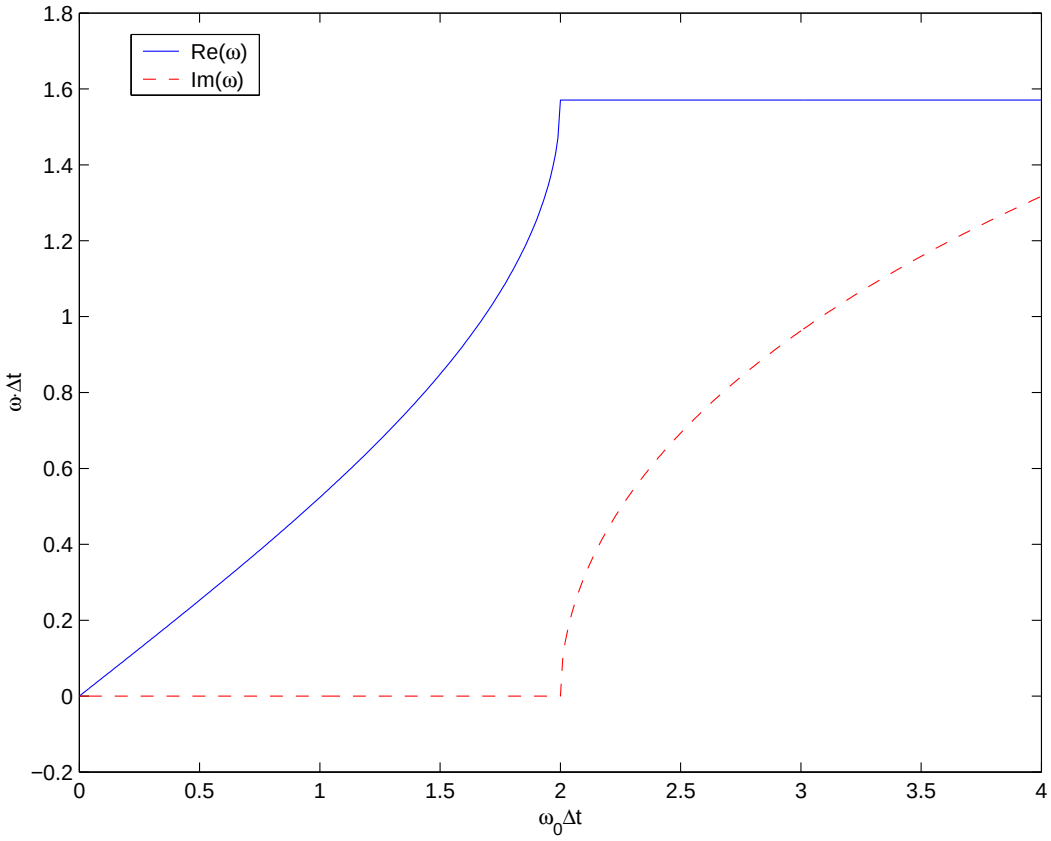

Figure 1.10: Effect of the finite time step for the leapfrog algorithm on the stability of the motion of a simple harmonic oscillator: ω and ω_0 denote the frequency of the simulation and of the harmonic oscillator, respectively ([1]).

particle balance (gain $\leq$ loss)

$$n_e \nu_{ion} V = \bar{n}_i n_n \sigma_{ion} v_{th} L A \approx \frac{n_i(SE)}{\lambda_{mfp}} \sqrt{\frac{k_B T_e}{m_e}} L A =\leq n_i c_S A \approx n_i \sqrt{\frac{k_B T_e}{m_i}} A,$$

leads to

$$L \leq \sqrt{\frac{m_e}{m_i}} \lambda_{mfp} \tag{1.36}$$

Here we took for simplicity $\bar{n}_i = n_i(SE)$, often $n_i(SE) = 0.5\bar{n}_i$.
For $B \neq 0$ additionally

$$\Delta t \leq \frac{0.35}{\omega_p}$$

must hold.

1.2.6.2 Particle Sources

BIT1 offers essentially two different kinds of particle sources: the sources may be located in the middle of the system and/or at one or both of the boundaries. The ion and electron particle fluxes in the source have to be prescribed accurately according to physical considerations to avoid artificial results.

Consider the case of the source being the right-hand boundary of the simulation region which is also assumed to be at the sheath edge. First of all at the sheath edge we have quasineutrality $n_i = n_e = n$. At the right-hand boundary we can only inject particles going to the left. So the incoming electrons are assumed to have a half Maxwellian electron distribution with formal temperature T_e, whose flux Γ_e is

$$\Gamma_e = \frac{n v_{th}}{\sqrt{2\pi}}, \quad \text{with } v_{th} = \sqrt{k_B T_e / m_e}$$

The Bohm criterion requires that the average ion velocity at the sheath edge is the ion sound velocity. Therefore we assume the ion distribution at the right-hand boundary to be a shifted Maxwellian distribution with shift velocity v_{shift} and a cut at $v \approx 0$: The shift velocity has to be chosen so that the mean ion velocity is just $-c_S$. This leads to

$$v_{\text{shift}} = -c_S + \sqrt{\frac{2}{\pi}} v_{th} e^{-v_{\text{shift}}^2 / 2 v_{th}^2} \left(1 + \frac{1}{\text{erf}(|v_{\text{shift}}| / \sqrt{2} v_{th})} \right)$$

With collisions the ion velocity distribution is not Maxwellian any more (Fig.1.11), so that setting up the flux is more complicated. One usually fixes the ion flux at the value $n v_{\text{shift}}$, where n is the density at the sheath edge (which is about half the density of the bulk plasma) and changes the input flux of the electrons to avoid unphysical properties at the source. Essentially one ensures quasineutrality, which can be diagnosed with the density profile, but even better with the profile of the electric field. The problem is that one really has to wait for steady state to judge the quality of the simulation. In order to save time the first trials can be made with a smaller number of computer particles.

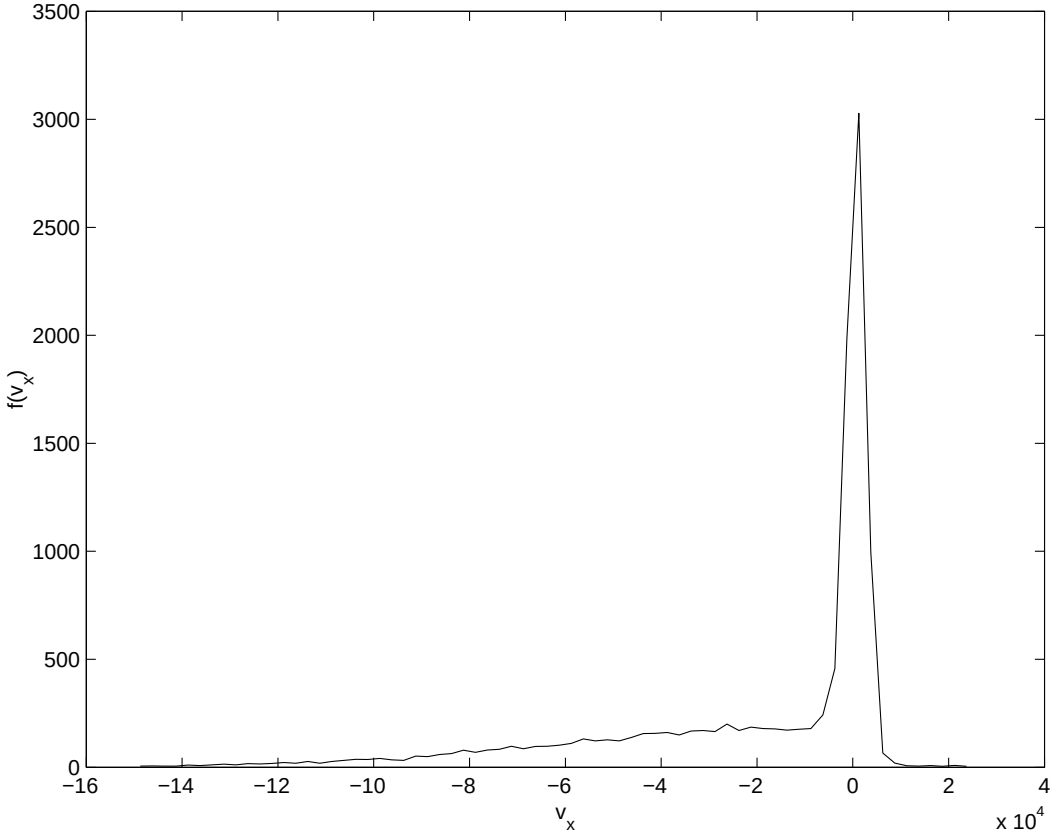

Figure 1.11: Velocity distribution of ions, when charged-neutral collisions are on.

Chapter 2

Theoretical calculation of the influence of secondary electrons on the stability of the PWT

Secondary electrons (SEs) are emitted from the wall due to the impact of primary particles (electrons or ions, but we will only consider electrons) on the wall. Then they get accelerated in the sheath and enter the presheath as a distinct beam with a narrow velocity distribution function. If the corresponding electron-beam instability is stronger than the damping processes in the presheath, the presheath becomes unstable. In this section we derive the dispersion relation, the numerical solution of which shows that we can expect an instability induced by the secondary electrons.

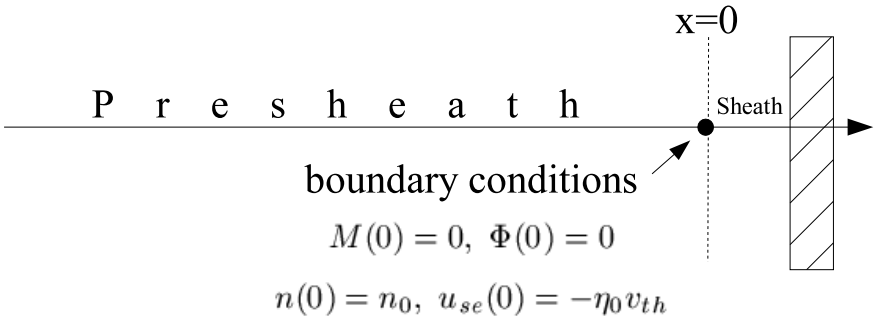

Figure 2.1: 1-D system considered for the calculation of a sufficient condition for presheath instability.

In this section we consider the 1-D system shown in Fig.2.1. The wall is at

$x = L$, the sheath-presheath boundary at $x = 0$ and the presheath corresponds to negative values of x. The main calculation refers to the presheath. The sheath influences the presheath solution by imposing the appropriate boundary conditions at the sheath-presheath boundary. The boundary of the plasma is not explicitly included because of the justification of section 1.1.4 where we showed that at least for the special case of the Pierce Diode for long enough systems the influence of the boundary on the stability properties of the plasma can be neglected. In what follows γ is the secondary electron emission coefficient, n_0 is the plasma density at the presheath entrance ($x = 0$), j is the current density, and $c_S = \sqrt{k_B(T_e + T_i)/m_i}$ is the ion sound velocity. Here, the difference of this value for c_S to the more general value (1.20) is very small (of the order of a few percent).

2.1 Sheath in the presence of secondary electrons

First we look at the sheath to get the appropriate boundary conditions for the calculation of the presheath instability.

The Bohm criterion is the starting point for this calculation since it provides a value for the ion particle flux density from a plasma to the surface. A brief investigation showed that it also holds for simulations including secondary electrons. However, a more detailed investigation will be done in the next future. Due to its small width we assume the sheath to be collisionless. Therefore the ion current entering the sheath (at $x = 0$) is the same as the ion current reaching the surface (at $x = L$),

$$|j_i(0)| = |j_i(L)| = en_0c_S.$$

We are now in a position to derive an expression for secondary electron emission from the surface, arising from electron impact, since this is significant even at rather modest energies, $T_e \geq 30eV$. Note that here and in what follows primary electrons will have the index e and secondary electrons will have the index se. By contrast, ion-induced secondary electron emission is usually only important for ion impact energies of $\geq 1keV$. By definition of the secondary electron coefficient γ the secondary electron current density is the fraction γ of the current density j_{pe} of the incoming primary electrons

$$|j_{se}(L)| = \gamma|j_e(L)|,$$

So the secondary electrons decrease the net electron current

$$|j_{e,\mathrm{tot}}(L)| = |j_e(L)| - |j_{se}(L)| = (1 - \gamma)|j_e(L)|,$$

For $j_e(L)$ we take the flux of a Maxwellian distribution flowing to a wall ([14, 15])

$$|j_e(0)| = |j_e(L)| = \frac{1}{4} e n_0 \sqrt{\frac{8}{\pi}} v_{th} \exp\left(\frac{e\Delta\phi}{k_B T_e}\right), \quad v_{th} = \sqrt{\frac{k_B T_e}{m_e}},$$

where $\Delta\phi < 0$ is the potential drop from the sheath edge to the wall. The total current at the sheath edge is given by

$$j(0) = j(L) =: j = |j_i(0)| - |j_{e,\mathrm{tot}}(0)|,$$

which directly leads to

$$\frac{e\Delta\phi}{k_B T_e} = \ln\left(\frac{\sqrt{2\pi}(c_S - j/en_0)}{(1-\gamma)v_{th}}\right). \tag{2.1}$$

The secondary electrons are accelerated by the sheath potential from the wall to the sheath edge and reach the velocity

$$|u_{se}(0)| = \sqrt{\frac{-2e\Delta\phi}{m_e}} = \sqrt{2} v_{th} \sqrt{\frac{-e\Delta\phi}{k_B T_e}}.$$

Using equation (2.1) this leads to

$$|u_{se}(x=0)| = \eta_0 v_{th}, \quad \eta_0 = \sqrt{2\ln\left(\frac{(1-\gamma)v_{th}}{\sqrt{2\pi}(c_S - j/en_0)}\right)} \gtrsim 1. \tag{2.2}$$

2.2 Presheath Model

The calculations below are based on the model given in [18]. We consider a plasma presheath with one ion species. As boundary condition at the sheath entrance ($x = 0$) we assume that the secondary electrons enter the presheath with a velocity u_{se} equal to or higher than the plasma electron thermal velocity (2.2). We additionally have as boundary conditions $\phi(x = 0) = 0$, quasineutrality ($n_i = n_e = n_0$) and the Bohm criterion $u_i = c_S$.

For the primary electron temperature T_e we assume the typical range $10eV \leq T_e \leq 100eV$. We assume that secondary electrons have zero velocity directly after their creation at the wall, so their energy spread is very small compared to the energy spread of the primary electrons. This condition allows us to use a cold-beam approximation for the secondary electrons. The computational part of this thesis suggests that a relaxation of this condition may be desirable, because the energy of the secondary electrons can spread due to the

induced instability. However this will be a future refinement of the theory. We also assume η_0 to be of order unity.

From section 1.1.5 we expect an oscillation frequency $\omega \approx k u_{se} \gtrsim k v_{th}$. The plasma electrons must be described with a kinetic model, whereas the ions and secondary electrons will be treated hydrodynamically.

Assuming isothermal ions and plasma electrons and neglecting terms of the order m_e/m_i, n_{se}/n_e and u_e/v_{th}, we write the following system of equations describing the plasma presheath. The system consists of the continuity and momentum equations for ions and secondary electrons, the kinetic equation for the plasma electrons and - since we only consider electrostatic waves - the Poisson equation.

$$\begin{aligned}
\frac{\partial}{\partial t} n_i + \frac{\partial}{\partial x} n_i u_i &= n_e \nu_{ion} \\
\frac{\partial}{\partial t} n_{se} + \frac{\partial}{\partial x} n_{se} u_{se} &= 0 \\
\frac{\partial}{\partial t} u_i + u_i \frac{\partial}{\partial x} u_i + \frac{e}{m_i} \frac{\partial}{\partial x} \phi &= -\frac{1}{m_i n_i} \frac{\partial}{\partial x} n_i k_B T_i - (\nu_{in} + \nu_{ion}) u_i - \nu_{ie}(u_i - u_e) \\
\frac{\partial}{\partial t} u_{se} + u_{se} \frac{\partial}{\partial x} u_{se} - \frac{e}{m_e} \frac{\partial}{\partial x} \phi &= -\nu_{se} u_{se} \qquad (2.3) \\
\frac{\partial}{\partial t} f_e(x,v) + v \frac{\partial}{\partial x} f_e(x,v) &+ \frac{e}{m_e} \frac{\partial \phi}{\partial x} \frac{\partial}{\partial v} f_e(x,v) = -\nu_e (f_e - f_0) \\
f_0(x,v) &= \frac{n_e^0(x)}{\sqrt{2\pi} v_{th}} \exp(-v^2/2v_{th}^2) \\
\frac{\partial^2}{\partial x^2} \phi &= \frac{e}{\epsilon_0}(n_e + n_{se} - n_i)
\end{aligned}$$

Here $n_e = \int f_e dv$, $u_e = n_e^{-1} \int v f_e dv$ and the ν's are the characteristic frequencies for different collisions (see [18] and Table 2.1). Λ is the Coulomb-logarithm: $10 \leq \Lambda \leq 18$. In the table, the temperature and density are given in eV and m^{-3}, respectively.

The right-hand side of the momentum equation for the secondary electrons is $\nu_{se} u_{se}$ and does not contain the difference between u_{se} and u_i or u_e, because u_{se} is much bigger than u_i and u_e, so u_i and u_e are neglected.

In order to use the cold-beam approximation for the secondary electrons we assume the friction to be sufficiently small:

$$\frac{\partial}{\partial x} u_{se} \sim \frac{u_{se}}{\delta x} \sim \frac{v_{th}}{\delta x} \gg \nu_{se}, \qquad (2.4)$$

where δx is the scale length of the presheath inhomogeneity.

ν	Collision accounts for	Formula	Value
ν_{ion}	electron impact ionization	$\sigma_{ion}(T_e, n_e)v_{th}n_n$	$6 \cdot 10^4$
ν_{in}	ion-neutral elastic and charge exchange	$\sigma_i v_{th} n_n$	10^5
ν_{ie}	ion-electron collision momentum transfer	$1.48 \cdot 10^{-12}\Lambda n m_e/m_i T_e^{3/2}$	50
ν_{se}^c	SE with ions and primary electrons	$2.41 \cdot 10^6 \Lambda n/\lvert u_{se}\rvert^3$	$2 \cdot 10^6$
ν_{se}^n	SE with neutrals (elastic+excitation)	$\langle \sigma_{el+ex} v\rangle n_n$	$6 \cdot 10^5$
ν_{se}	SE with ions, primary electrons, neutrals	$\nu_{se}^c + \nu_{se}^n$	$3 \cdot 10^6$
ν_e	elastic collisions of plasma electrons	$5 \cdot 10^{-12}\Lambda n T_e^{3/2}$	$3 \cdot 10^5$

Table 2.1: Formulas and typical values for collision frequencies for $n = 10^{18}\mathrm{m}^{-3}, n_n = 10^{19}\mathrm{m}^{-3}$, $T_e = 30\mathrm{eV}$, $T_i = 15\mathrm{eV}, \Lambda = 10$ and Hydrogen ions.

2.3 Zeroth order solution

Now we make an ansatz

$$\Theta(x,t) = \Theta^0(x) + \Theta^1(x)e^{i(\omega t - kx)},\ \Theta^0 \gg \Theta^1,\ k \gg \frac{\partial}{\partial x}\ln\Theta^{0,1}, \tag{2.5}$$

where Θ denotes the physical quantities $n_{e,i,se}$, $u_{e,i,se}$, f_e entering the basic equations. Now we will insert the ansatz (2.5) into the model, retain zero-order terms and obtain the system describing the presheath in the time-independent state. First we define

$$M := u_i^0/c_S,\ \nu_{sum} := \nu_{ion} + \nu_{in},\ \text{and } a := \sqrt{\frac{\nu_{ion}+\nu_{in}}{\nu_{ion}}}.$$

(i) Densities: We start with the 0^{th} order equation for the primary electrons,

$$\frac{\partial}{\partial t}f_e^0 + v\frac{\partial}{\partial x}f_e^0 + \frac{e}{m_e}\frac{\partial\phi^0}{\partial x}\frac{\partial}{\partial v}f_e^0 = -\nu_e(f_e^0 - f_0)$$

Substituting $f_e^0 = f_0$ in this equation leads to

$$\frac{\partial n_e^0(x)}{\partial x} = \frac{e}{m_e}\frac{\partial\phi^0}{\partial x}n_e(x)/v_{th}^2.$$

Dividing by $n_e^0(x)$, integrating over x and taking the exponential of the result we obtain

$$n_e^0(x) = n_0 \exp\left(\frac{e\Phi}{k_B T_e}\right). \tag{2.6}$$

Assuming approximate quasineutrality in 0^{th} order means that $n_i^0(x) = n_e^0(x) =: n^0(x)$. The total current to the wall, which is the same as the current at the sheath edge, consists of the ion and the electron part

$$j = n_i^0 u_i^0 - j_e(wall) = n_0 c_S - (1-\gamma) j_{e,wall} = n_0 c_S - \frac{1-\gamma}{\gamma} j_{se}.$$

Thus, using $j_{se} = -e n_{se}^0 v_{se}^0 = e n_{se}^0 \eta_0 v_{th}$,

$$n_{se}^0 = \frac{1-\gamma}{\gamma} \frac{n_0 c_S - j}{\eta_0 v_{th}}.$$

(ii) Ion velocity: Starting with the 0^{th}-order ion momentum equation

$$u_i^0 \frac{\partial u_i^0}{\partial x} + \frac{e}{m_i} \frac{\partial \phi^0}{\partial x} = -\frac{T_i}{m_i n} \frac{\partial n^0}{\partial x} - \nu_{sum} u_i^0,$$

we substitute $\partial\phi^0/\partial x$ by n using the Boltzmann relation (2.6), to obtain

$$u_i^0 \frac{\partial u_i^0}{\partial x} + \frac{c_S^2}{n^0} \frac{\partial n^0}{\partial x} = -\nu_{sum} u_i^0. \tag{2.7}$$

We can express $\partial n^0/\partial x$ by terms including u_i^0 using the continuity equation, yielding

$$(u_i^0 - \frac{c_S^2}{u_i^0}) \frac{\partial u_i^0}{\partial x} + \frac{c_S^2 \nu_{ion}}{u_i^0} = -\nu_{sum} u_i^0.$$

This is a differential equation with separated variables. Thus we multiply by u_i^0, put the terms with u_i^0 on the left side and the rest on the right side, and integrate:

$$\int_{u_{i,0}^0}^{u_i^0} \frac{u^2 - c_S^2}{c_S^2 \nu_{ion} + \nu_{sum} u^2} du = \frac{c_S}{\nu_{ion}} \int_1^M \frac{\tilde{M}^2 - 1}{1 + \tilde{M}^2 \nu_{sum}/\nu_{ion}} d\tilde{M} = -\int_0^x d\tilde{x} = -x \tag{2.8}$$

To evaluate the integral on the left-hand side we first make the substitution $z = M\sqrt{\nu_{sum}/\nu_{ion}} =: aM$ and rewrite it in the form

$$\frac{c_S}{\nu_{ion}} \frac{1}{a^2} \int_a^{aM} \frac{z^2 - a^2}{1 + z^2} \frac{d\tilde{z}}{a} = \frac{c_S}{\nu_{ion}} \frac{1}{a^3} \int_a^{aM} \frac{(1+z^2) - (1+a^2)}{1+z^2} d\tilde{z}$$

Evaluating this and combining it with the right-hand side of (2.8) leads to

$$M - 1 - \left(\frac{1}{a} + a\right) (\arctan((aM) - \arctan(a)) = -\frac{a^2 \nu_{ion}}{c_S} x = -\frac{\nu_{sum}}{c_S} x.$$

(iii) Potential: We start with equation (2.7) in the form

$$u_i^0 \frac{\partial u_i^0}{\partial x} + c_S^2 \frac{\partial}{\partial x} \ln(n^0) = -\nu_{sum} u_i^0$$

and the continuity equation

$$0 = \frac{1}{n^0} \frac{\partial}{\partial x}(n^0 u_i^0) - \nu_{ion} = u_i^0 \frac{\partial}{\partial x} \ln(n^0) + \frac{\partial u_i^0}{\partial x} - \nu_{ion}.$$

In order to remove the term $-\nu_{sum} u_i^0$, we multiply the former equation by ν and the latter equation by $\nu_{sum} u_i$, and add both equations to obtain

$$(c_S^2 \nu_{ion} + \nu_{sum} u_i^2) \frac{\partial}{\partial x} \ln(n^0) = -(\nu_{ion} + \nu_{sum}) u_i^0 \frac{\partial u_i^0}{\partial x} = -\frac{1}{2}(\nu_{ion} + \nu_{sum}) \frac{\partial (u_i^0)^2}{\partial x}.$$

So

$$\frac{\partial}{\partial x} \ln(n^0) = -\frac{1}{2}(\nu_{ion} + \nu_{sum}) \frac{\partial M^2 / \partial x}{\nu_{ion} + \nu_{sum} M^2}.$$

Now we get ϕ using the Boltzmann equation

$$\phi = \frac{k_B T_e}{e} \ln(n^0) = \frac{k_B T_e}{e} \int_{x_0}^{x} \frac{\partial}{\partial x} \ln(n^0) dx = \frac{k_B T_e}{e} \frac{\nu_{ion} + \nu_{in}/2}{\nu_{sum}} \ln\left(\frac{\nu_{ion} + \nu_{sum} M_0}{\nu_{ion} + \nu_{sum} M^2} \right).$$

Note, that the boundary condition $\phi^0(x = 0) = 0$ is fulfilled for $M_0 = M(x = 0) = 1$.

Summary: (time-independent state)
The 0^{th}-order solution of the model (2.3) *with the boundary conditions*

$$\phi^0(x = 0) = 0, \quad M(x = 0) = 1, \quad u_{se}^0(x = 0) = -\eta_0 v_{th}$$

has the following form:

$$\begin{aligned}
f_e^0(x, v) &= f_0(x, v) \\
n_i^0 = n_e^0 =: n &= n_0 \exp\left(\frac{e\phi^0}{k_B T_e} \right) \\
1 - \frac{\nu_{sum}}{c_S} x &= M - \left(a + \frac{1}{a} \right) (\arctan(aM) - \arctan(a)) \\
\phi^0 &= \frac{k_B T_e}{e} \frac{\nu_{ion} + \nu_{in}/2}{\nu_{sum}} \ln\left(\frac{2\nu_{ion} + \nu_{in}}{M^2 \nu_{sum} + \nu_{ion}} \right) \qquad (2.9) \\
n_{se}^0 &= \frac{\gamma}{1 - \gamma} \frac{n_0 c_S - j/e}{\eta_0 v_{th}} \\
u_{se}^0 \frac{\partial}{\partial x} u_{se}^0 &= -\frac{e}{m_e} \frac{\partial}{\partial x} \phi^0 - \nu_{se} u_{se}^0
\end{aligned}$$

for

$$f_0(x,v) = \frac{n_e^0(x)}{\sqrt{2\pi}v_{th}} \exp(-v^2/2v_{th}^2),\ \nu_{sum} = \nu_{ion} + \nu_{in}$$

and

$$a = \sqrt{\frac{\nu_{ion} + \nu_{in}}{\nu_{ion}}},\ M = u_i^0/c_S,\ c_S = \sqrt{\frac{k_B T_e}{m_i}}.$$

The 0^{th}-order solution (2.9) has the following structure. The electron and ion density, $n_e^0(x)$ and $n_i^0(x)$, are both given by the Boltzmann term $\exp(e\phi/k_B T_e)$ (thus we have quasineutrality in the presheath), the electrons being Maxwellian. The ion velocity $u_i^0(x)$ is given by an implicit equation. The potential ϕ^0 is also space-dependent ($\phi^0 = \phi^0(M(x))$).

The velocity of the secondary electrons is still given by the differential equation

$$u_{se}^0 \frac{\partial}{\partial x} u_{se}^0 = -\frac{e}{m_e}\frac{\partial}{\partial x}\phi - \nu_{se} u_{se}^0 \tag{2.10}$$

which, however, can be solved numerically because ϕ^0 is now known. Fig.2.2 shows the numerical solution of the differential equation for u_{se} for various secondary-electron emission coefficients γ. We obtained the solution using the simple explicit Adams method [9]). In each step of the Adams method in order to evaluate $\phi^0(x)$ we have to obtain $M(x)$ from the equation

$$1 - \frac{\nu_{sum}}{c_S} x = M - \left(a + \frac{1}{a}\right)(\arctan(aM) - \arctan(a)) \tag{2.11}$$

and insert this into (2.9), so that we obtain $\phi^0(x) = \phi^0(M(x))$. In our simulations the wall is at the left side. For easier comparisons with simulations in Fig.2.2 the presheath is in the positive halfspace and the presheath entrance is at $x = 0$.

We see that $|u_{se}^0|$ increases monotonically from the sheath-presheath boundary (x=0). For increasing γ the value of $|u_{se}^0|$ decreases and reaches the minimal value for $\gamma_c = 0.81$. The value γ_c is the critical value (for a hydrogen plasma), for which in the sheath no monotonic solution for ϕ exists ([5]).

A good approximation for the maximum value at the end of the presheath is

$$|u_{se}^0|_{max}/v_{th} \approx \sqrt{\eta_0^2 + \frac{2\nu_{ion} + \nu_{in}}{\nu_{ion} + \nu_{in}} \ln(2 + \nu_{in}/\nu_{ion})}. \tag{2.12}$$

To obtain this result we make the following approximation in the differential equation for u_{se}^0 (2.10), which can be made because of the weak friction

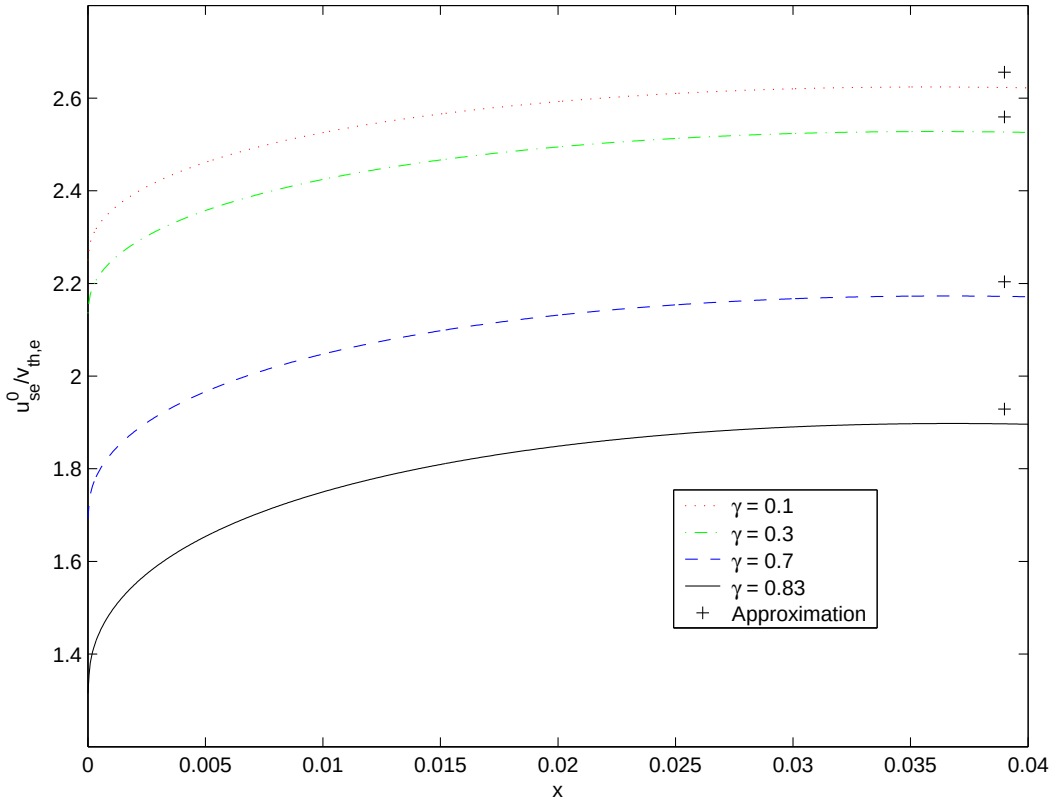

Figure 2.2: Numerical solution for the secondary-electron velocity for various secondary electron emission coefficients γ.

condition (2.4),

$$u^0_{se}\frac{\partial}{\partial x}u^0_{se} = \frac{1}{2}\frac{\partial}{\partial x}(u^0_{se})^2 = -\nu_{se}u^0_{se} + \frac{e}{m_e}\frac{\partial}{\partial x}\phi^0 \approx \frac{e}{m_e}\frac{\partial}{\partial x}\phi^0,$$

from which we obtain

$$(u^0_{se})^2_{max} = u^0_{se}(-L)^2 \approx u^0_{se}(0)^2 + \int_0^{-L}\frac{2e}{m_e}\frac{\partial\phi^0}{\partial x}dx \approx \eta_0^2 v_{th}^2 + \frac{2e\phi^0(-L)}{m_e}, \quad (2.13)$$

where we already used $\phi^0(x=0)=0$. From equation (2.9) we find $\phi^0(x=-L)=\phi^0(M=0)$

$$\phi^0(x=-L) = \frac{k_B T_e}{e}\frac{\nu_{ion}+\nu_{in}/2}{\nu_{sum}}\ln\left(\frac{2\nu_{ion}+\nu_{in}}{\nu_{ion}}\right).$$

Substitution of $\phi^0(-L)$ in (2.13) leads to (2.12). Formula (2.12) holds very well (Fig.2.2). For later use we note that $\eta \geq 1.3$ holds everywhere in our system.

2.4 First-order solution

The next step consists in solving the time-independent first-order equations. We first derive the dispersion relation which we then approximately solve for the region near the end of the presheath, to obtain a sufficient condition for the presheath instability.

(i) We start out with the first-order Poisson equation,

$$\frac{\partial^2}{\partial x^2}\phi^1 e^{i(\omega t-kx)} = -k^2\phi^1 = \frac{e}{\epsilon_0}(n_e^1 + n_{se}^1) \tag{2.14}$$

Note that in deriving this equation we have neglected certain terms in accordance with the assumption $k \gg \frac{\partial}{\partial x}\Theta^{0,1}$.
(ii) Now we insert the appropriate expressions for the densities into the Poisson equation (2.14). The secondary-electron density n_{se}^1 is found from the first-order continuity and momentum equations for the secondary electrons. The former equation has the form

$$\frac{\partial}{\partial t}n_{se}^1 e^{i(\omega t-kx)} + \frac{\partial}{\partial x}\left(n_{se}^0 u_{se}^1 e^{i(\omega t-kx)} + n_{se}^1 e^{i(\omega t-kx)} u_{se}^0\right) = 0$$

which leads to

$$n_{se}^1 = \frac{k n_{se}^0 u_{se}^1}{\omega - k u_{se}^0}. \tag{2.15}$$

As before we have neglected some terms involving $\partial\Theta^{0,1}/\partial x$. Before inserting this term into Poissons equation we calculate u_{se}^1 from the first-order momentum equation

$$\begin{aligned} -\nu_{se} u_{se}^1 e^{i(\omega t-kx)} &= \frac{\partial}{\partial t}u_{se}^1 e^{i(\omega t-kx)} + u_{se}^0 \frac{\partial}{\partial x}u_{se}^1 e^{i(\omega t-kx)} \\ &\quad + u_{se}^1 e^{i(\omega t-kx)}\frac{\partial}{\partial x}u_{se}^0 + \frac{e}{m_e}\frac{\partial}{\partial x}\phi^1 e^{i(\omega t-kx)}. \end{aligned}$$

Neglecting terms proportional to $\partial\Theta^{0,1}/\partial x$ as before and performing the derivatives we find

$$u_{se}^1 = -\frac{ke}{m_e}\phi^1/(\omega - k u_{se}^0 - i\nu_{se}).$$

Substituting u_{se}^1 in equation (2.15) we obtain the desired equation for n_{se}^1 (note that $u_{se}^0 < 0$, so we can write $|u_{se}^0|$ instead of $-u_{se}^0$)

$$n_{se}^1 = -k^2\phi^1 \frac{e n_{se}^0/m_e}{(\omega + k|u_{se}^0|)(\omega + k|u_{se}^0| - i\nu_{se})}.$$

Now we substitute the expression found for the first-order secondary-electron density and the first-order primary-electron density

$$n_e^1 = \int dv f_e^1$$

in Poisson's equation (2.14) to obtain

$$-k^2\phi^1 = \frac{e}{\epsilon_0}\left(\int dv f_e^1 - k^2\phi^1 \frac{en_{se}^0/m_e}{(\omega + k|u_{se}^0|)(\omega + k|u_{se}^0| - i\nu_{se})}\right)$$

Using the definition of the plasma frequency ω_p and defining

$$\alpha := \frac{n_{se}^0}{n^0}$$

we can rewrite this as

$$\phi^1 = \phi^1 \frac{\alpha\omega_p^2}{(\omega + k|u_{se}^0|)(\omega + k|u_{se}^0| - i\nu_{se})} - \frac{e}{\epsilon_0 k^2}\int dv f_e^1 \tag{2.16}$$

(iii) In the last step we have to treat the primary electron term using the first-order kinetic equation for the electrons

$$\begin{aligned} -\nu_e f_e^1 e^{i(\omega t - kx)} &= \frac{\partial}{\partial t} f_e^1 e^{i(\omega t - kx)} + v\frac{\partial}{\partial x} f_e^1 e^{i(\omega t - kx)} \\ &+ \frac{e}{m_e}\frac{\partial f_e^0}{\partial v}\frac{\partial}{\partial x}\phi^1 e^{i(\omega t - kx)} + \frac{e}{m_e}\frac{\partial \phi^0}{\partial x}\frac{\partial}{\partial v} f_e^1 e^{i(\omega t - kx)} \end{aligned}$$

Neglecting terms with $\partial\Theta^{0,1}/\partial x$ and taking the derivatives we find

$$(\omega - kv - i\nu_e) f_e^1 = \frac{ek}{m_e}\frac{\partial f_e^0}{\partial v}\phi^1$$

Now we can solve this equation for f_e^1 and substitute the latter in equation (2.16),

$$1 = \frac{\alpha\omega_p^2}{(\omega + k|u_{se}^0|)(\omega + k|u_{se}^0| - i\nu_{se})} - \frac{e^2}{\epsilon_0 k m_e}\int dv \frac{\partial f_e^0/\partial v}{\omega - kv - i\nu_e} \tag{2.17}$$

(iv) Now we focus on the term with the integral. Substituting f_e^0 and differentiating with respect to v, yields

$$\frac{e^2}{\epsilon_0 k m_e}\frac{n_e(x)}{\sqrt{2\pi}v_{th}v_{th}^2}\int dv \frac{v\exp(-v^2/2v_{th}^2)}{\omega - kv - i\nu_e}.$$

On simplifying the constants in front of the integral and multiplying the nominator and denominator by $-k$ we find

$$-\frac{1}{k^2\lambda_D^2}\frac{1}{\sqrt{2\pi}v_{th}}\int dv\frac{[(\omega-kv-i\nu_e)+(-\omega+i\nu_e)]\exp(-v^2/2v_{th}^2)}{\omega-kv-i\nu_e}.$$

In the second term we make the substitution $t=v/\sqrt{2}v_{th}$, which leads to

$$-\frac{1}{k^2\lambda_D^2}\frac{1}{\sqrt{2\pi}v_{th}}\left(\sqrt{2}v_{th}\int dte^{-t^2}+\frac{\omega-i\nu_e}{\sqrt{2}kv_{th}}\sqrt{2}v_{th}\int dt\frac{\exp(-t^2)}{t-(\omega-i\nu_e)/\sqrt{2}kv_{th}}\right).$$

The first integral is well known to be $\sqrt{\pi}$, the second is equal to $\sqrt{\pi}Z((\omega-i\nu_e)/\sqrt{2}kv_{th})$, so we can write it as

$$-\frac{1}{k^2\lambda_D^2}\left(1+\frac{y}{\sqrt{2}}Z\left(\frac{y}{\sqrt{2}}\right)\right)$$

with

$$y:=\frac{\omega-i\nu_e}{kv_{th}}.$$

Summary (dispersion relation):
Collecting terms of first order in the system (2.3) *one obtains the dispersion relation*

$$1=\frac{\alpha\omega_p^2}{(\omega+k|u_{se}^0|)(\omega+k|u_{se}^0|)-i\nu_{se}}-\frac{1}{k^2\lambda_D^2}\left(1-J_+\left(\frac{\omega-i\nu_e}{kv_{th}}\right)\right) \quad (2.18)$$

with

$$\alpha:=n_{se}^0/n,\quad J_+(y)=-\frac{y}{\sqrt{2}}Z\left(\frac{y}{\sqrt{2}}\right),\quad Z(y)=\frac{1}{\sqrt{\pi}}\int\limits_{-\infty}^{\infty}\frac{1}{t-y}e^{-t^2}dt.$$

A purely numerical treatment of the dispersion relation using the "pseudoarclength" continuation method ([4]) shows the following unstable solution branch (Fig.2.3).

Equation (2.18) can be considered as a dispersion relation only if the homogeneous plasma approximation is valid, i.e., the characteristic time of instability growth $1/|\mathrm{Im}(\omega)|$ is much smaller than the time the wave packet needs to "feel" the plasma inhomogeneity ($\delta x/u_{gr}$):

$$|\mathrm{Im}\omega|\gg\frac{1}{\delta x}\frac{\partial\omega}{\partial k}\sim\frac{\nu_{in}+\nu_{ion}}{c_S}|u_{se}^0|\sim(\nu_{in}+\nu_{ion})\eta\sqrt{\frac{m_i}{2m_e}} \quad (2.19)$$

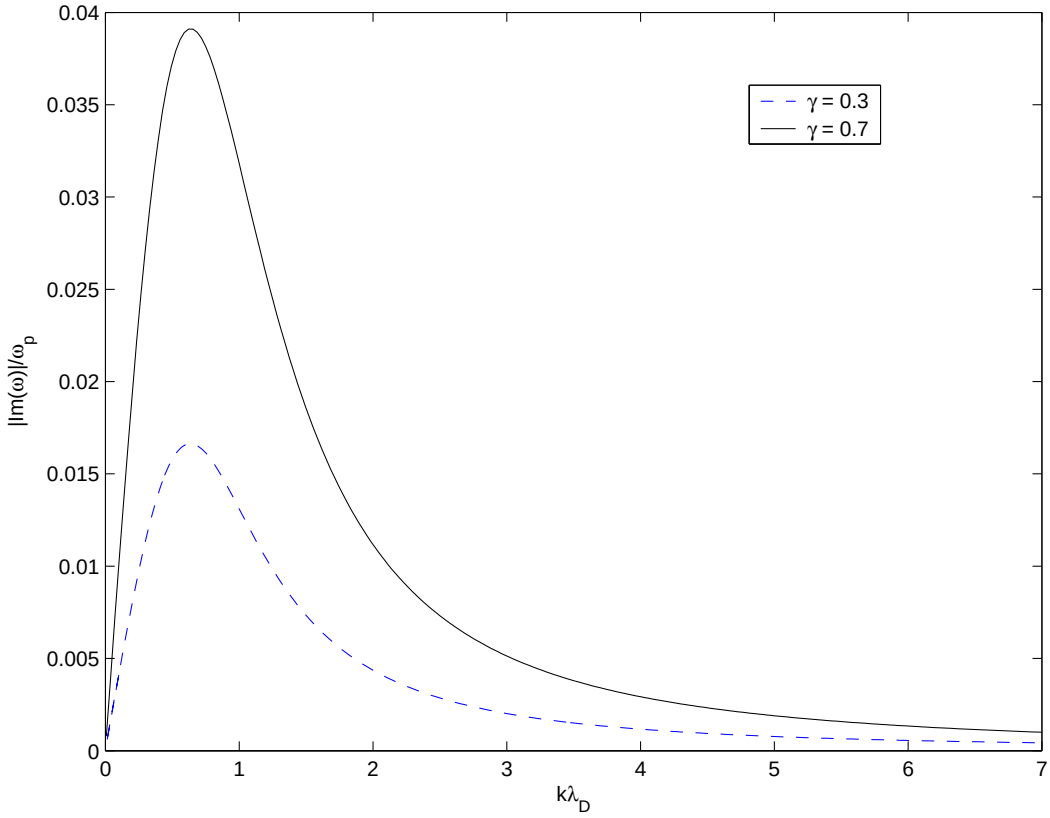

Figure 2.3: Numerical solution for the growing branch of the dispersion relation (2.18) for various values of γ.

Let us now take a closer look at the dispersion relation. Using the weak-friction (2.4) and the homogeneity condition (2.19) we will obtain a sufficient condition for the presheath instability.

We first want to find an expression for the imaginary part of the growing solution of (2.18). Multiplying the dispersion relation (2.18) by the denominator leads to

$$[(\omega + k|u_{se}^0|)^2 - i\nu_{se}(\omega + k|u_{se}^0|)][1 + (1 - J_+(y))/k^2\lambda_D^2] = \alpha\omega_p^2$$

Solving this quadratic equation for $\omega + k|u_{se}^0|$ we obtain

$$\omega \approx ku_{se}^0 + i\frac{\nu_{se}}{2} \pm \sqrt{\frac{\alpha\omega_p^2}{1 + (1 - J_+(y))/k^2\lambda_D^2} - \frac{\nu_{se}^2}{4}}. \tag{2.20}$$

Next we derive an expression for the imaginary part of the growing solution

of (2.20)

$$\mathrm{Im}(\omega) = \frac{\nu_{se}}{2} \pm \mathrm{Im}\left(\sqrt{\frac{\alpha\omega_p^2}{1+(1-J_+(y))/k^2\lambda_D^2} - \frac{\nu_{se}^2}{4}}\right). \tag{2.21}$$

To do this we must to find an expression for a term having the form $\mathrm{Im}(\sqrt{c+ib})$. On one hand

$$\sqrt{c+ib}^2 = c+ib,$$

on the other hand

$$\sqrt{c+ib}^2 = (\mathrm{Re}(\sqrt{c+ib}) + \mathrm{Im}(\sqrt{c+ib}))^2 = \mathrm{Re}^2 - \mathrm{Im}^2 + 2i\mathrm{ReIm}.$$

Comparing the imaginary parts we obtain $\mathrm{Re} = b/2\mathrm{Im}$. Substituting Re in the equation resulting from the comparison of the real parts we find

$$\left(\mathrm{Im}^2\right)^2 + c\mathrm{Im}^2 - b^2/4 = 0.$$

Solving this quadratic equation for Im^2 and taking the square root we obtain

$$\mathrm{Im} = \pm\frac{1}{\sqrt{2}}\sqrt{-c \pm \sqrt{c^2+b^2}}.$$

If $c > 0$ (we will show later that $c > 0$ holds) we must take the plus sign in front of the second root to get a real number because $\sqrt{c^2+b^2} > |c|$. This yields

$$\mathrm{Im} = \pm\frac{1}{\sqrt{2}}\sqrt{-c + \sqrt{c^2+b^2}}. \tag{2.22}$$

Multiplying the denominator of the fraction term of the root of (2.21) with its conjugate complex we can identify c with $-\nu_{se}^2/4 - \alpha\omega_p^2 A$ and b with $-\alpha\omega_p^2 B$ for

$$A := \frac{k^2\lambda_D^2(\mathrm{Re}J_+(y) - 1 - k^2\lambda_D^2)}{(\mathrm{Re}J_+(y) - 1 - k^2\lambda_D^2)^2 + (\mathrm{Im}J_+(y))^2}$$

and

$$B := \frac{k^2\lambda_D^2\mathrm{Im}J_+(y)}{(\mathrm{Re}J_+(y) - 1 - k^2\lambda_D^2)^2 + (\mathrm{Im}J_+(y))^2}.$$

Using equation (2.22) with c and b above equation (2.21) results in

$$\mathrm{Im}(\omega) = \frac{\nu_{se}}{2} \pm \frac{1}{\sqrt{2}}\sqrt{\frac{\nu_{se}^2}{4} + \alpha\omega_p^2\left(A\sqrt{\left(\frac{\nu_{se}^2}{4\alpha\omega_p^2} + A\right)^2 + B^2}\right)}$$

Due to the inhomogeneity and weak friction assumptions we can neglect ν_{se} because

$$\mathrm{Im}(\omega) \gg \frac{1}{\partial x}\frac{\partial\omega}{\partial k} \sim \frac{|u_{se}^0|(\nu_{in}+\nu_{ion})}{c_S} \sim \eta\frac{m_i}{m_e}(\nu_{in}+\nu_{ion}) \sim \nu_{se}.$$

Since we are searching for instabilities with $\mathrm{Im}(\omega) < 0$ we must take the minus sign in front of the root. Therefore we obtain

$$\mathrm{Im}(\omega) \approx -\frac{\sqrt{\alpha}\omega_p}{\sqrt{2}}\sqrt{A + \sqrt{A^2 + B^2}}. \tag{2.23}$$

For typical values (such as $k\lambda_D = 0.65$ (Fig.2.3) and $\mathrm{Re}(y) \approx 1.3$ (Fig.2.2) and small $\mathrm{Im}(y)$) A is negative which means that $c > 0$. Using (2.23) the homogeneity condition (2.19) can be written as

$$C_I := \frac{\sqrt{\alpha}\omega_p\sqrt{A + \sqrt{A^2 + B^2}}}{\eta\sqrt{m_i/m_e}(\nu_{in} + \nu_{ion})} \gg 1. \tag{2.24}$$

To find out if we can expect an instability we can numerically solve the dispersion relation (now with ν_{se} neglected) in order to obtain $\omega(k\lambda_D)$. Then we calculate $A(y(\omega(k\lambda_D)))$ and $B(y(\omega(k\lambda_D)))$ as functions of $k\lambda_D$ and insert it in (2.24) (Fig.2.4). Figure 2.4 shows that we can expect an instability induced by the secondary electrons for $k\lambda_D$ slightly less than 1.

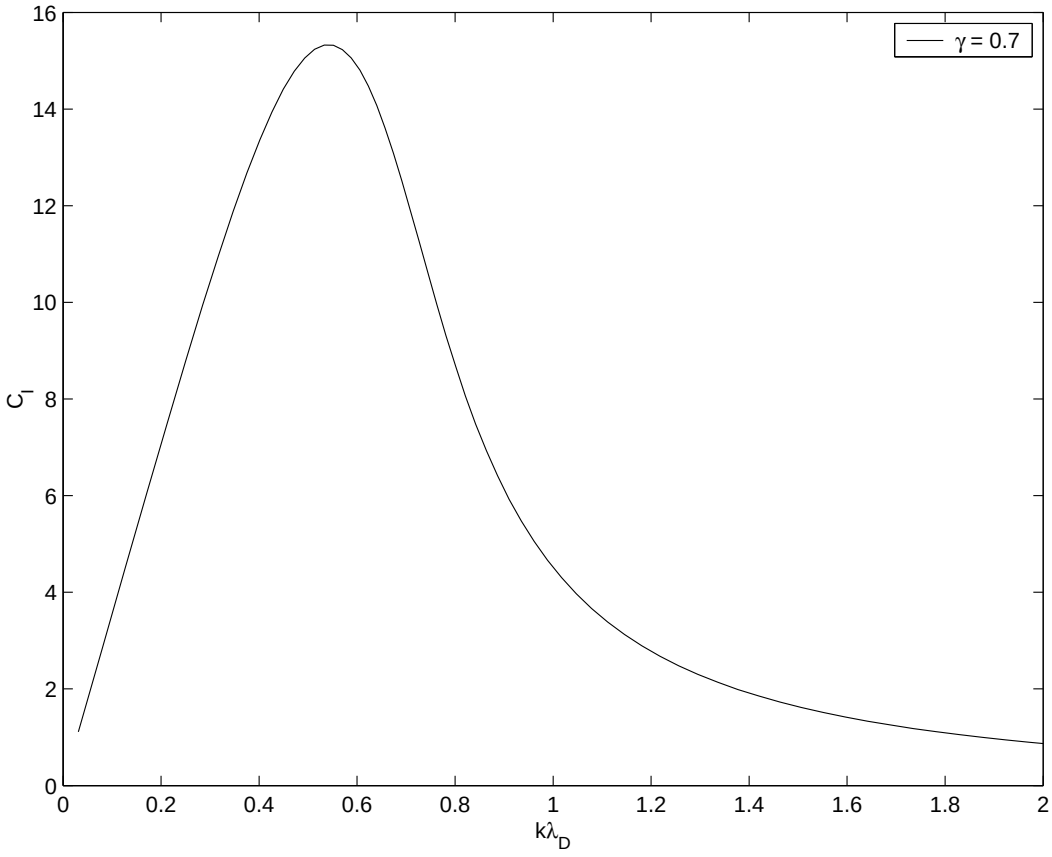

Figure 2.4: Instability criterion: for $C_I \gg 1$ we expect instability.

Chapter 3

Simulations

In this section we compare the results of the theory with results from simulations performed with BIT1. We will demonstrate in the simulation the instability which is induced by the secondary electrons. Based on the simulation results we additionally propose a mechanism which limits the growth of the instability.

3.1 Simulation Setup

The simulations were all done with the same version of the BIT1 code. The parameters are chosen so as to satisfy the conditions of section 1.2.6.1. A source on the right-hand boundary injects the particles (Fig.3.1). Note that in the simulation the wall is not at the left-hand side (as in the model) but at the right-hand side because more diagnostics are available at the left wall.

For the ion and electron particle fluxes entering at the right-hand boundary we first calculated

$$\Gamma_{R,i} = \frac{nv_{th,i}}{\sqrt{2\pi}} \text{ and } \Gamma_{R,e} = \frac{nv_{th,e}}{\sqrt{2\pi}}$$

and then adjusted the electron particle flux to ensure quasineutrality at the right-hand side. Every output is averaged over 4096 time steps corresponding to about 115 plasma oscillations $\nu_p = \omega_p/2\pi$. In the input-file of the code the particle species used in the simulation are defined by their masses, charges, input conditions et cetera. The simulations treat the secondary electrons in the same way as the primary electrons. For the purpose of obtaining all the

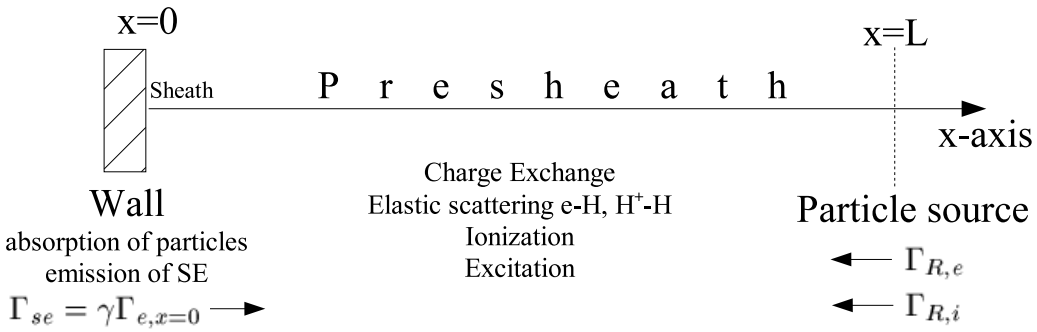

Figure 3.1: Simulation region.

diagnostics for the secondary electrons (especially their mean velocity and their velocity distribution) we additionally had to perform simulations where they were treated as a separate species.

The most important parameters of the simulation are given in table 3.1.

variable	description	value
nc	number of cells	400
nc2p	number of real particles per computer particle	$8 \cdot 10^6$
dt	time step	$3.5 \cdot 10^{-12}$
L	length of the system	0.02 m
area	area of the system	10^{-4} m
nfft	number of time steps for the FFT	4096
n_n	neutral density	$4 \cdot 10^{19}\ m^{-3}$
T_n	temperature of neutrals	0.001 eV
$\Gamma_{R,e}$	Electron injection flux at the right wall	$7.7 \cdot 10^{23}$
$T_{R,e}$	temperature of injected electrons	30 eV
$\Gamma_{R,i}$	Ion injection flux at the right wall	$2.14 \cdot 10^{22}$
$T_{R,i}$	temperature of injected ions	30 eV

Table 3.1: Description of the most important input parameters

The final simulations included about 200000 electrons and 200000 ions. With $\gamma = 0.7$, about 6800 secondary electrons were in the simulation, which means 17 secondary electrons per cell.

3.2 Basic Plasma Parameters

In this section we look at the influence of the secondary electrons on the basic plasma parameters such as density, potential, electric field, temperature and mean velocities. Figures 3.2 and 3.3 show that, in accordance with the theoretical results, in the presheath the basic plasma parameters do not change with changing secondary-electron emission coefficient γ. This does not hold for the sheath (Fig.3.4), where the potential drop is observed to depend on γ. Comparing in table 3.2 the value for the potential drop obtained from the simulation (the sheath edge was taken as the position where the plasma gets quasineutral) with the theoretical values [5] given in equation (3.1), we find good agreement between theory and simulation

$$-\frac{e\Delta\Phi}{k_B T_e} = \ln\left(\frac{1-\gamma}{\sqrt{2\pi m/M}}\right). \tag{3.1}$$

γ	$e\Delta\Phi/k_BT_e$ from (3.1)	$e\Delta\Phi/k_BT_e$ from simulation
0	2.84	2.87
0.3	2.48	2.52
0.7	1.64	1.64

Table 3.2: Potential drop in the presheath from theory and from simulation

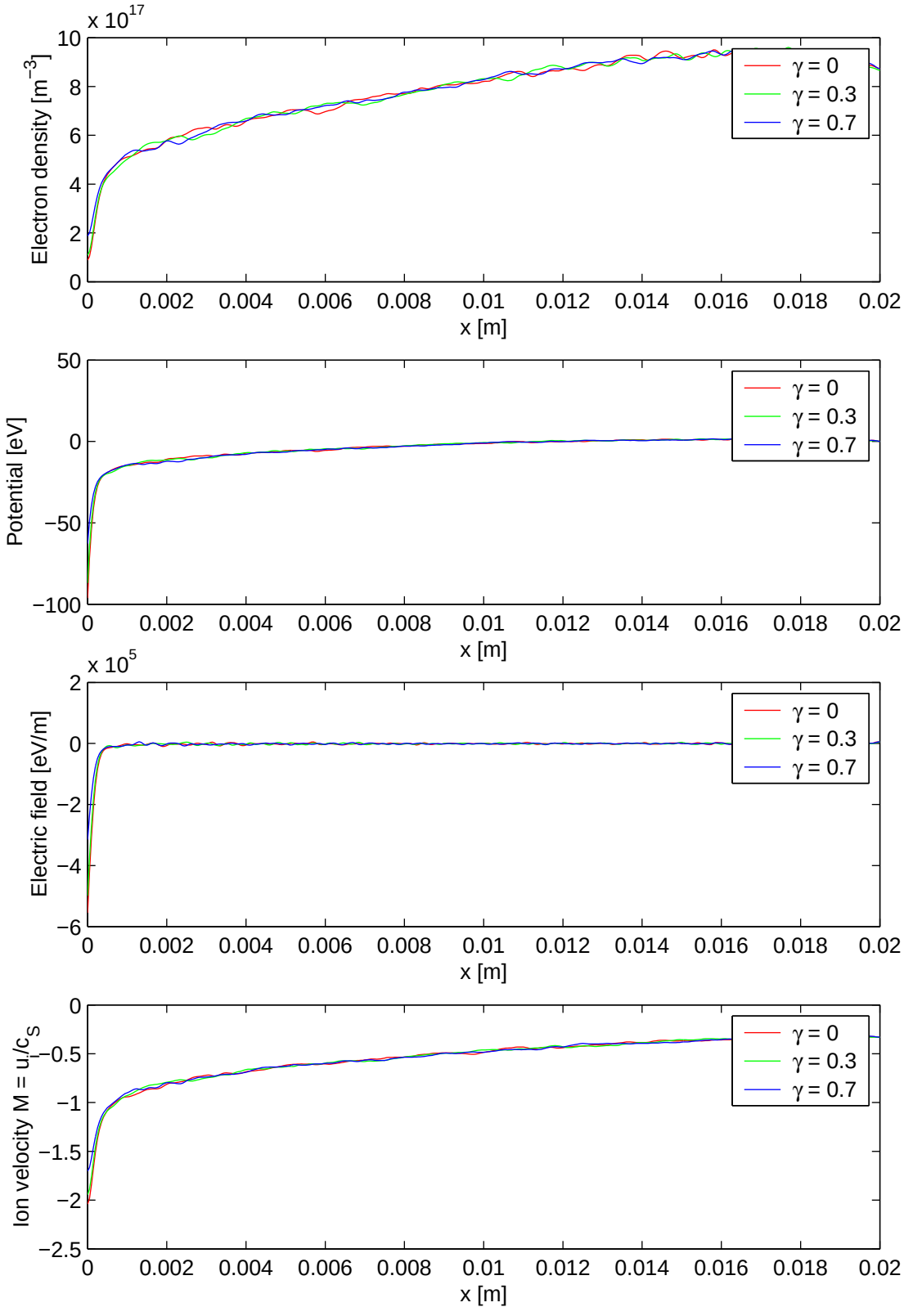

Figure 3.2: Density, potential, electric-field and ion-velocity profiles for the whole simulation region.

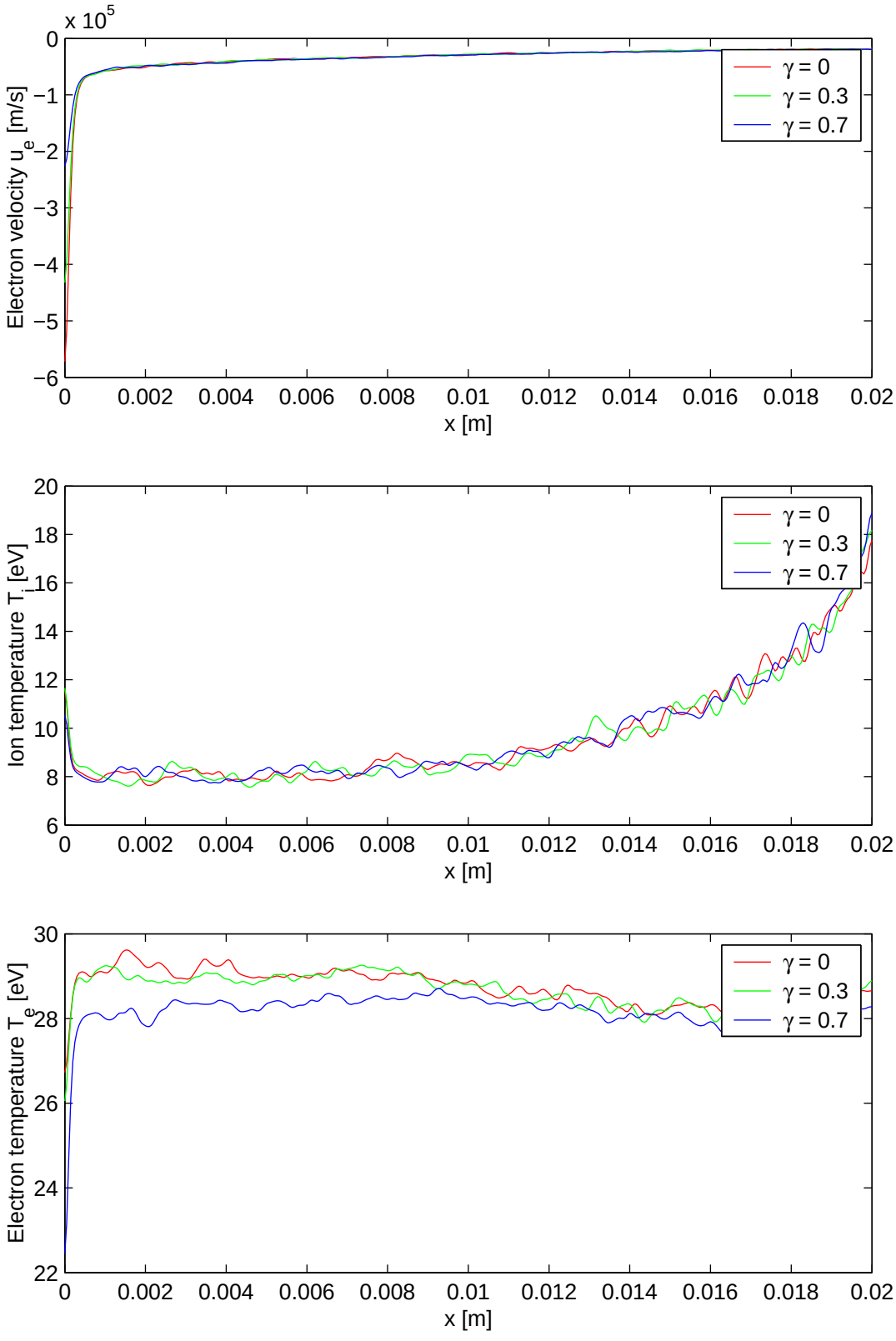

Figure 3.3: Electron-velocity, electron-temperature and ion-temperature profiles for the whole simulation region.

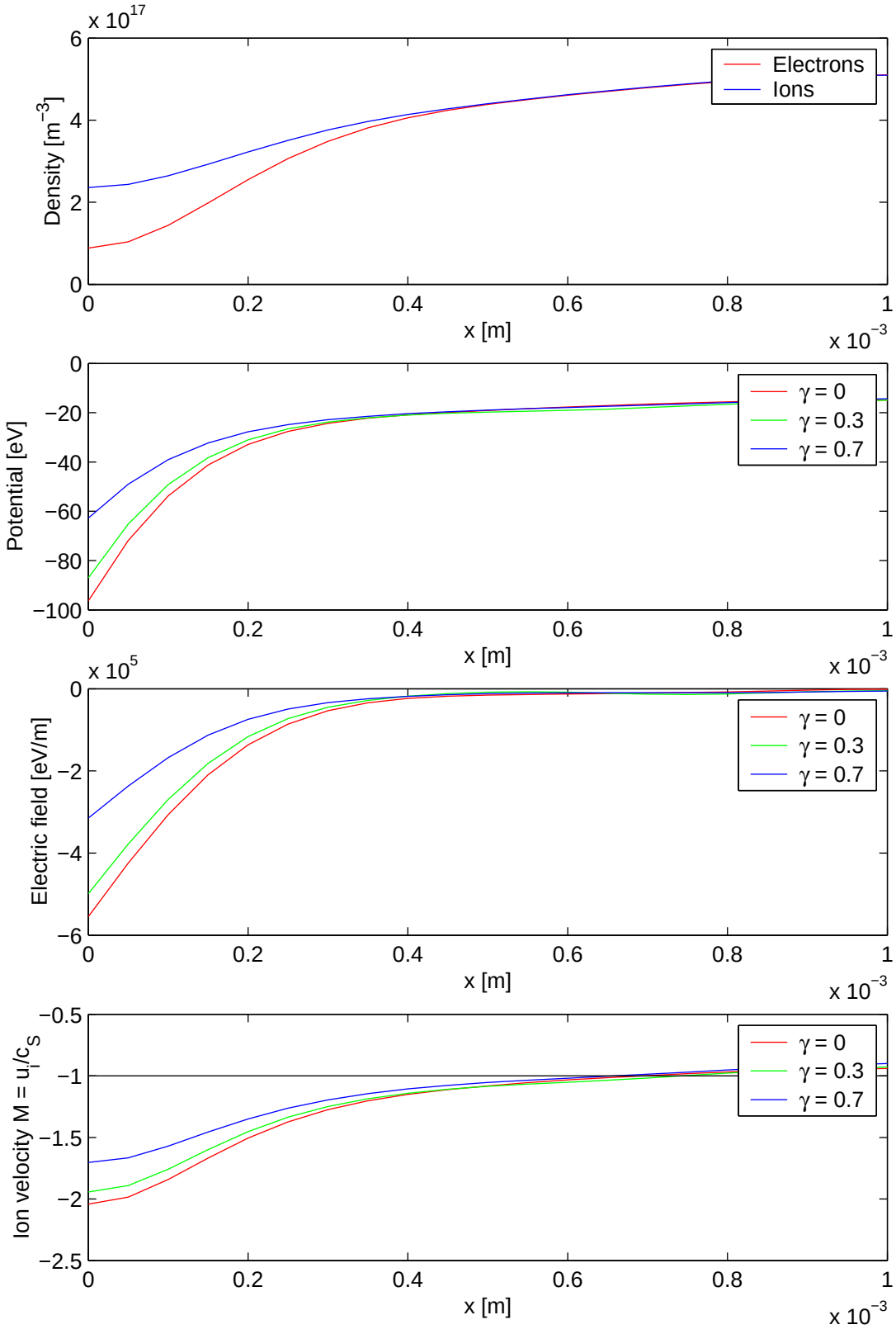

Figure 3.4: Density, potential, electric-field and ion-velocity profiles in the sheath region.

3.3 Check of the zeroth order model

In this section we compare the simulation results with those of the zeroth-order model (2.9).

There clearly are some differences between theory and simulation. The first difference concerns the ion temperature. As specified in the input-file the ions injected at the right boundary are not cold (Fig.3.3), the ion-temperature depends on the position x. The electron and ion densities depend on the position as well. Consequently the collision frequencies, which mostly depend on the temperature and/or the density become space-dependent, too. Even if these collision frequencies were not dependent on x, it would still not be straightforward to compare them with the collision frequencies of the model because the collision frequencies of the model account for the momentum transfer, whereas those of the code account for the number of collisions.

To compare model and simulation we take the collision frequencies of the simulation as first guesses and then vary them slightly manually for the purpose of fitting the mean ion-velocity profile ($M(x)$) using (2.11). Then we obtain the potential and density profile in a stepwise manner. Using (2.9) we find the potential profile $\phi^0(x) = \phi^0(M(x))$. Substituting $\phi^0(x)$ in the Boltzmann relation (2.6) we then obtain the density profile $n^0(x) = n^0(\phi^0(M(x)))$. To distinguish differences coming from the current step to differences from all the previous steps we additionally make hybrid models. There we use the mean ion velocity of the simulation instead of the mean ion velocity of the model and the potential of the simulation instead of the potential of the model in step two and three, respectively.

For the mean ion velocity we get a rough fit (Fig.3.5, upper panel) which is good at the sheath-side and gets worse in the direction of the right-hand boundary. This is not surprising because the use of (2.11) ensures that the mean ion velocity is equal to the sound velocity at the sheath edge. Surprisingly in the next step this rough fit for the mean ion velocity leads to very good agreement with the potential obtained from the simulation (Fig.3.5, middle panel). The fit is even better than the fit where we used the mean ion velocity obtained from the simulation. The potential of the simulation has a slight decrease at the right wall which is more likely a source effect of the simulation. The lowest panel of Fig.3.5 shows that in the last step the density profile can be excellently predicted by the Boltzmann relation using the potential profile obtained from the simulation. Also the pure model works quite well. At the right wall again the source effect can be identified.

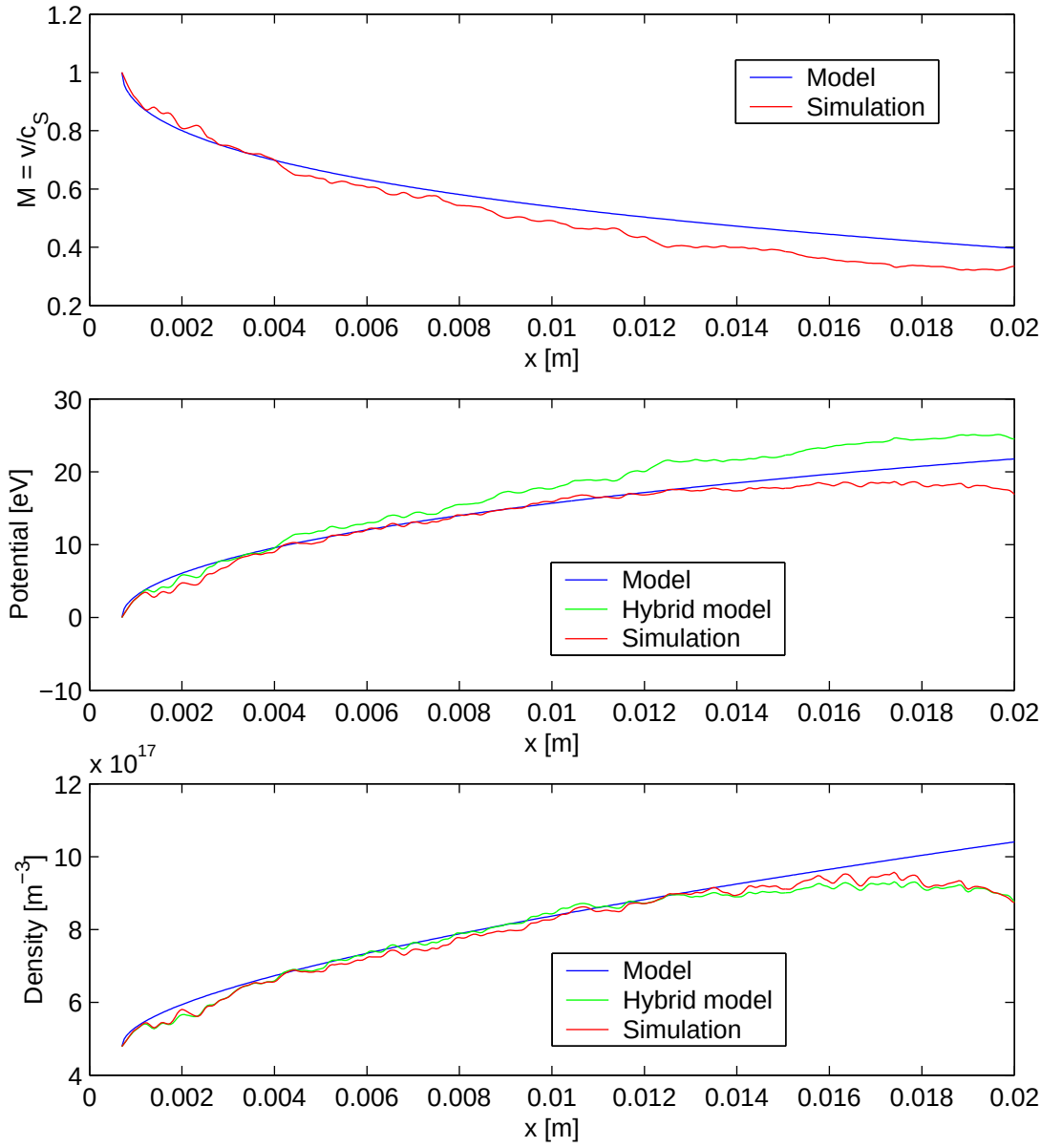

Figure 3.5: Comparison of theory with simulations. Density, potential, ion-velocity and secondary-electron-velocity profiles. The hybrid model for the potential uses the ion velocity from the simulation in equation (2.9), the hybrid model for the density uses the potential obtained from the simulation in Boltzmann's relation (2.6).

Figure 3.6 shows a comparison of the mean velocity of the secondary electrons obtained from the simulation with the velocity obtained from the numerical solution of the differential equation (2.10). The mean secondary electron velocity for both simulation and numerical solution increases entering the presheath at the sheath edge. However, while the numerical solution continues to increase, u_{se}^0 taken from the simulation decreases. We account this lack of fit to the instability which is induced by the secondary electron beam. We will see later (Fig.3.13) that also the temperature of the secondary electrons increases during the penetration of the presheath. This happens approximately at the same position where the numerical solution and the simulation begin to show different behaviours regarding u_{se}^0.

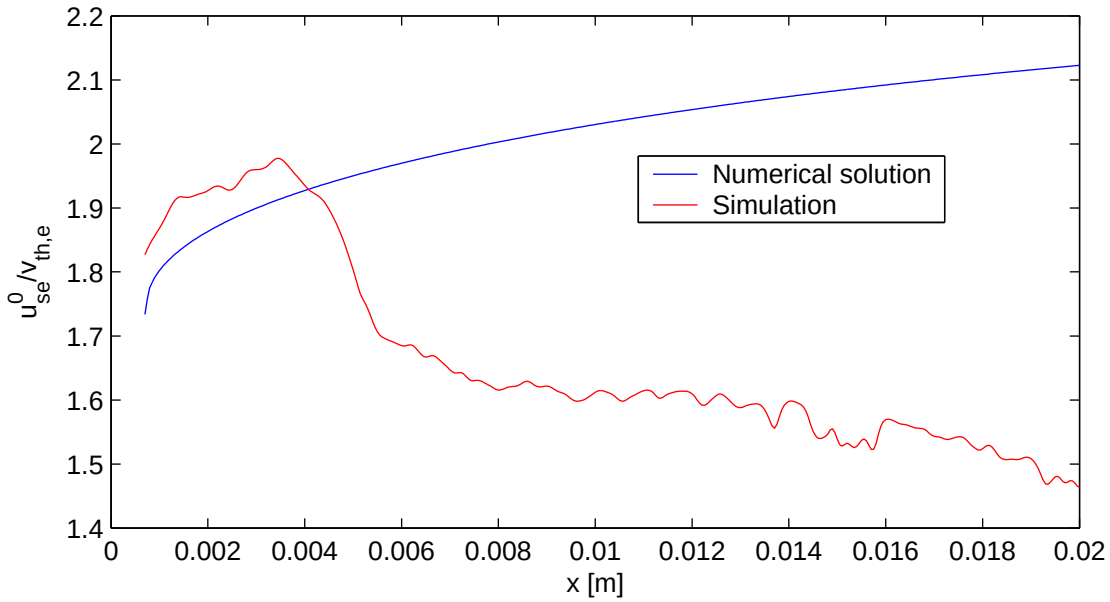

Figure 3.6: Mean velocity of secondary electrons u_{se}^0 obtained from the simulation and from the numerical solution of differential equation (2.10) (both for $\gamma = 0.7$).

Figure 3.7 shows that the electrons are approximately Maxwellian distributed.

In contrast to the electrons the ion-velocity distribution is clearly not Maxwellian (Fig.3.8) due to collisions (especially due to charge exchange collisions with the cold neutral background). At the position $x = 0.0018$ which is still inside the presheath the ions are already clearly accelerated by the potential of the presheath.

In Fig.3.9 we check the density of the secondary electrons (2.9) which should only depend on γ (not on x). We plot $\alpha := n_{se}^0/n_0$ dependent on γ and

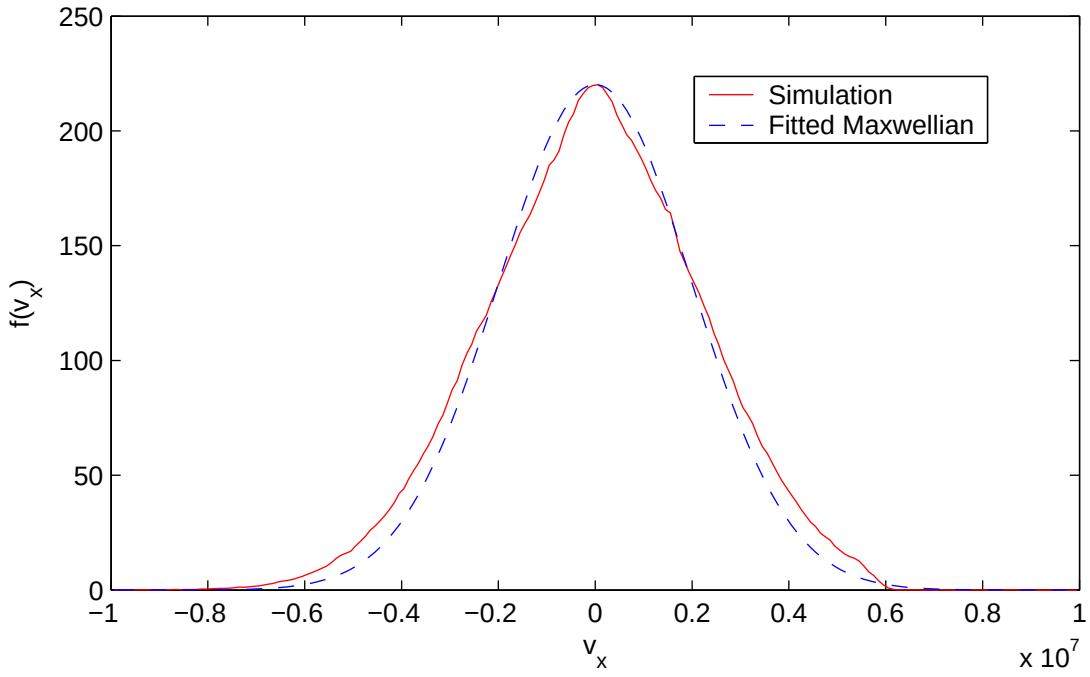

Figure 3.7: Electron-velocity distribution.

compare the result with the simulations performed with $\gamma = 0.3$ and $\gamma = 0.7$. In the simulation the secondary electron density is not constant but slightly depends on x. Therefore we plot a bar from the minimum to the maximum value of the secondary electron density and obtain good agreement with (2.9).

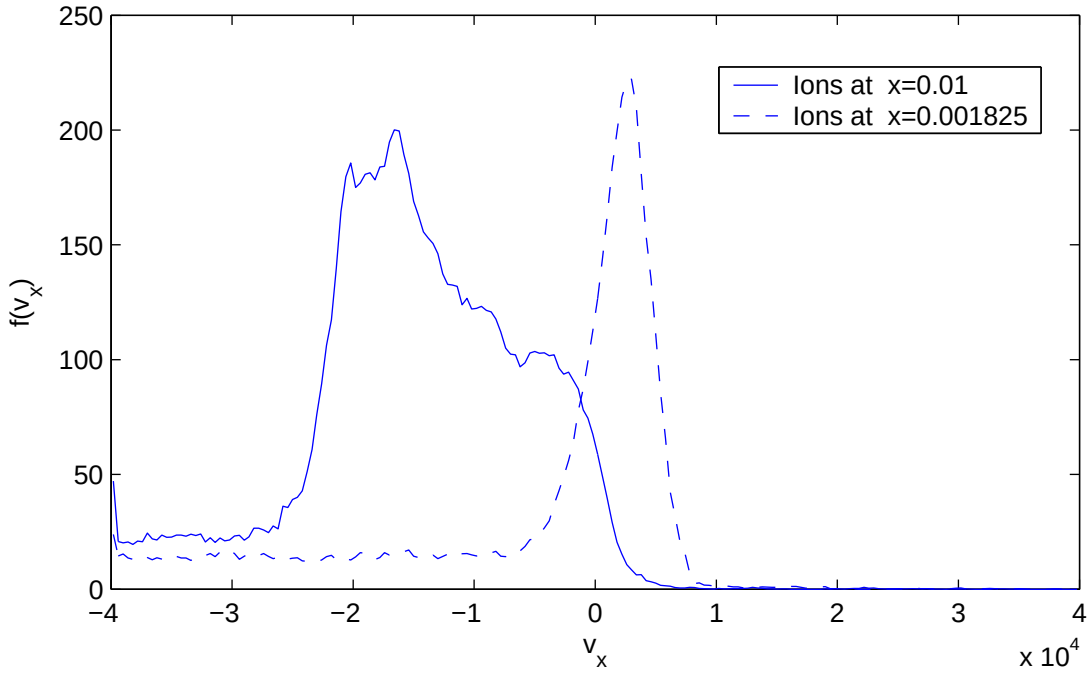

Figure 3.8: Ion-velocity distribution at two different positions in the presheath.

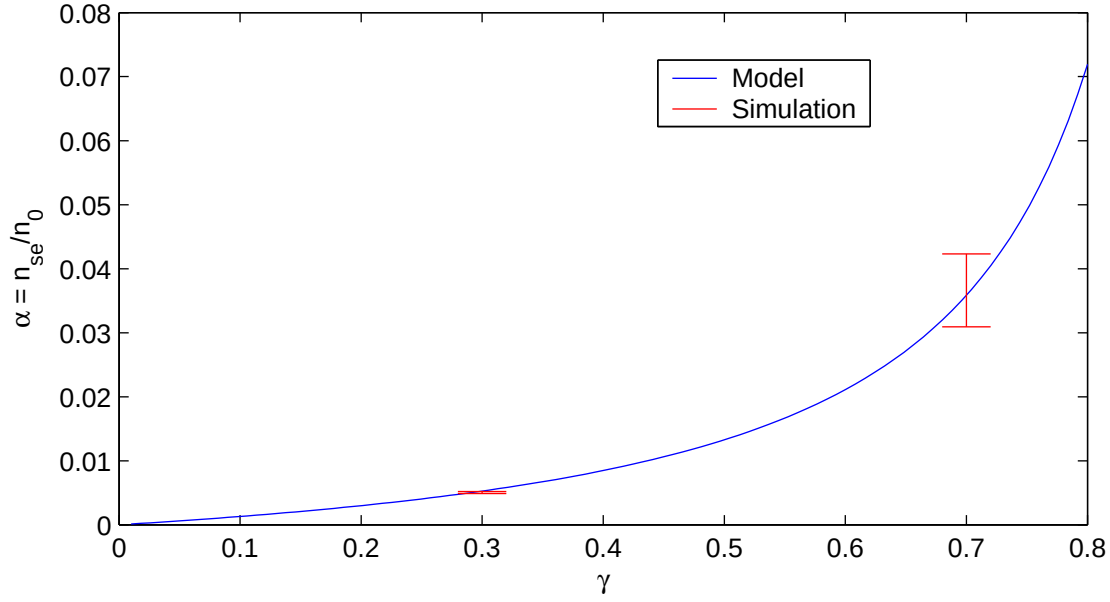

Figure 3.9: Comparison of theory with simulations. Density of the secondary electrons dependent on the secondary electron emission coefficient γ.

3.4 Instability

3.4.1 Detection of the Instability

In this section we demonstrate the instability in the simulation. For this purpose we look at the frequency spectrum of the potential at two different positions (Fig.3.10). We clearly see that the peak which is near the plasma frequency is increasing with increasing secondary electron emission coefficient γ.

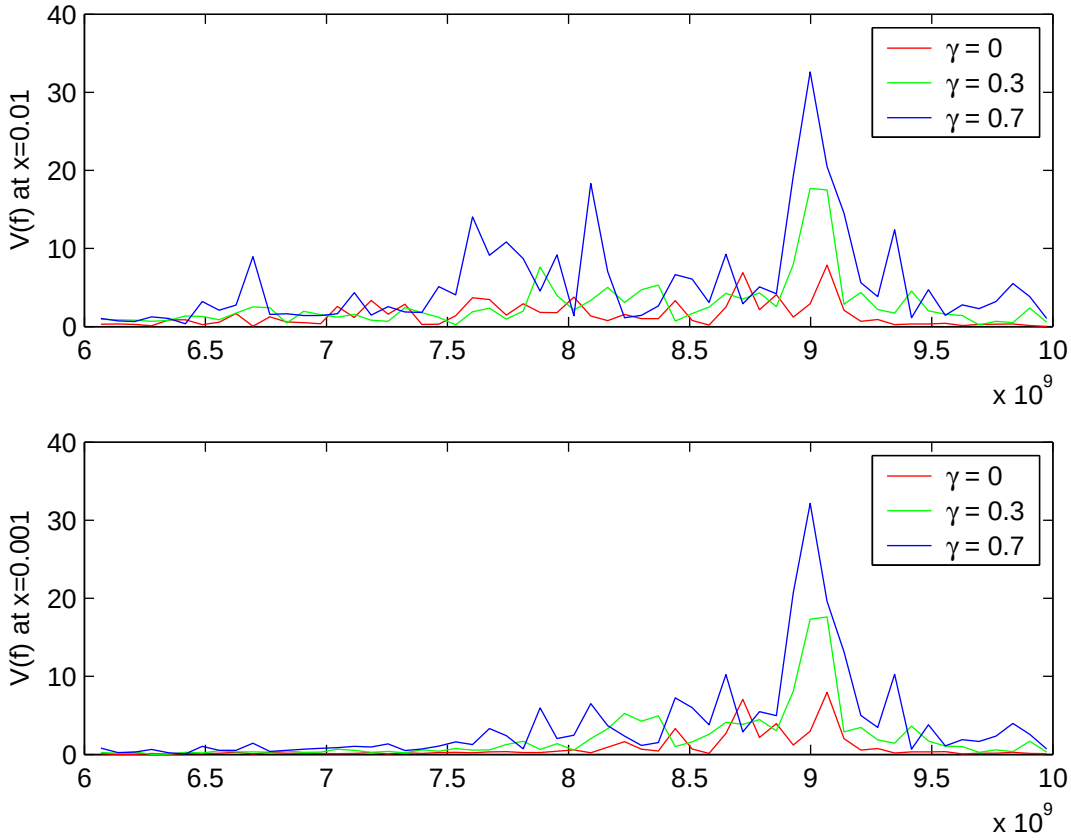

Figure 3.10: Instability induced by secondary electrons for two different values of the secondary electron emission coefficient γ for two different positions.

To ensure that the instabilities shown in Fig.3.10 do not have numerical reasons we did the same simulations with four times more computer particles (800000 per species). Also in these simulations the instability could be demonstrated (Fig.3.11). The instability for $\gamma = 0.3$ can be identified even better than in the simulation using fewer computer particles.

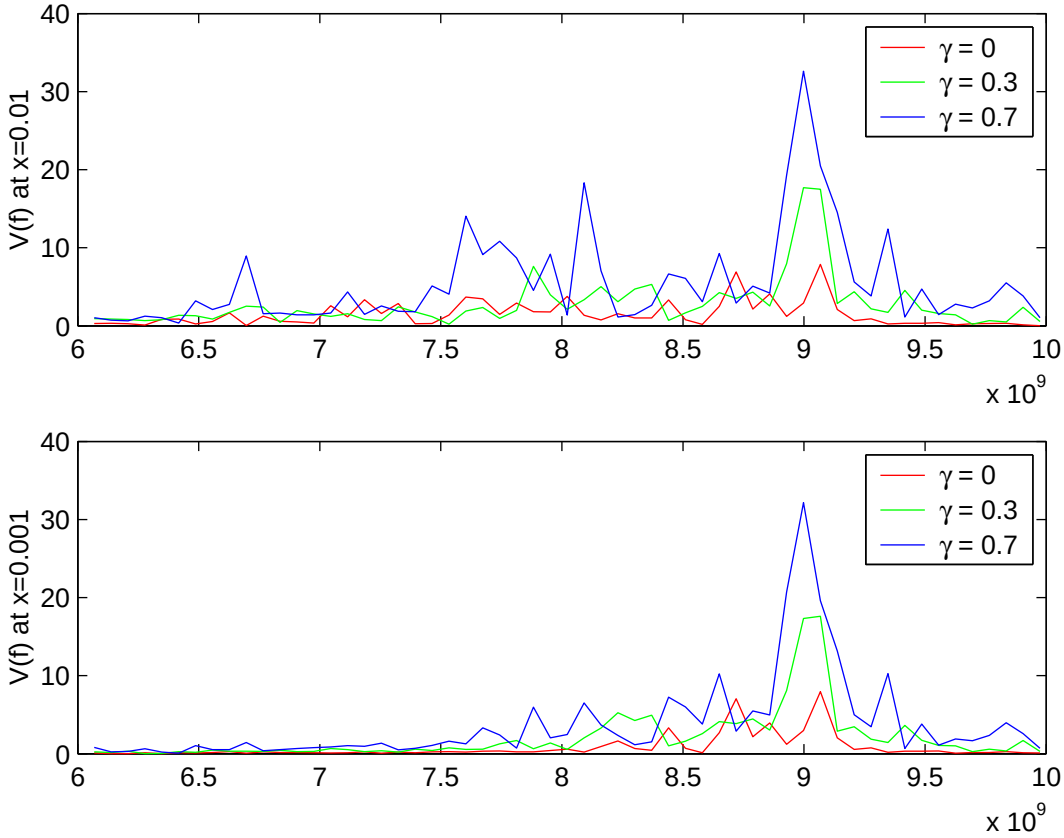

Figure 3.11: Instability induced by secondary electrons for two different values of the secondary electron emission coefficient γ for two different positions for the simulation with four times more simulation particles.

3.4.2 Saturation of the Instability

3.4.2.1 The Penrose criterion

Let us look at the mechanism which we conjecture to be responsible for stopping the growth of the instability. As the starting point for the explanation we state the Penrose criterion (Fig.3.12) [2].

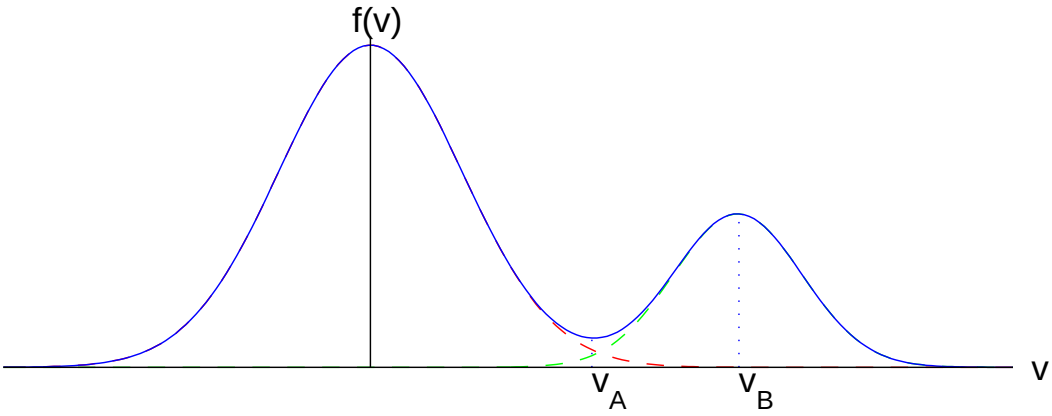

Figure 3.12: Penrose criterion: beam-plasma distribution function.

The Penrose criterion asserts that the condition

$$\int_{-\infty}^{\infty} \frac{f(v) - f(v_A)}{(v - v_A)^2} dv > 0$$

is a necessary and sufficient criterion for instabilities. The existence of a minimum of the electron velocity distribution is not, of itself, a sufficient criterion for instability. In effect, the minimum must be deep enough. However, in our case it turned out that even a very shallow minimum is sufficient for the development of an instability.

The Penrose criterion is not directly applicable to our system because it considers the collisionless case with ions treated as a homogeneous background. However, it can be viewed as an approximative instability-treatment. The Penrose criterion will give us a hint how the growth of the instability is stopped.

3.4.2.2 The saturation mechanism

Examining the diagnostics of the runs with three species we observed that the temperature of the secondary electrons strongly depends on the position x (Fig.3.13). We conjectured that the observed temperature rise could affect the result of the application of the Penrose criterion.

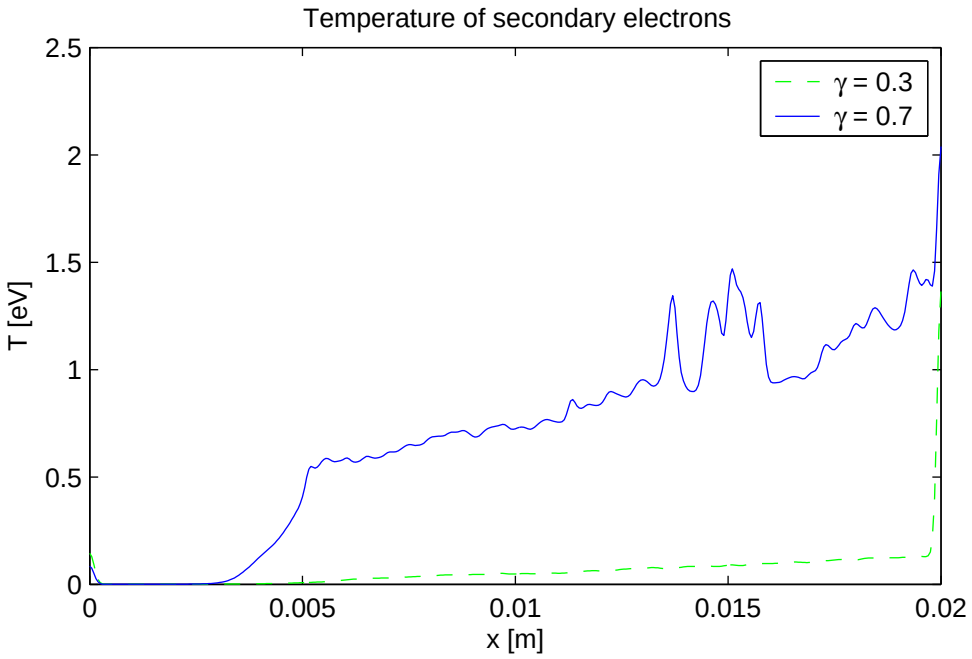

Figure 3.13: Secondary-electron-temperature profile for two different values of the secondary electron emission coefficient γ.

To apply the Penrose criterion we consider the total electron velocity distribution consisting of the primary electron distribution and the secondary electron distribution. If the system contains enough cold and fast secondary electrons the total distribution should have a minimum. Penetrating the presheath the secondary-electron-temperature rises and their velocity distribution flattens leading to a shallower minimum of the total-electron-velocity distribution. When the minimum is shallow enough the Penrose criterion is not fulfilled any more and the instability saturates. To examine this behavior in the simulations we compared the total electron distribution for several positions and observed the expected behavior of the total electron distribution (Fig.3.14).

Note again that the Penrose criterion is not directly applicable to our system.

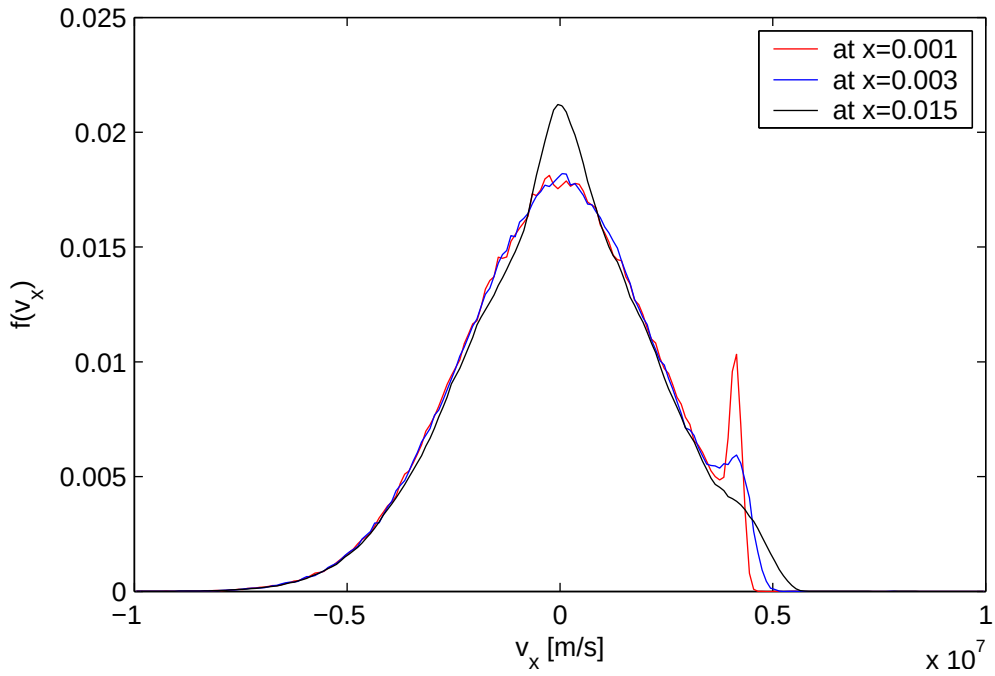

Figure 3.14: The consequence of the flattening of the secondary-electron-velocity distribution for the total-electron-velocity distribution for $\gamma = 0.7$.

Therefore in the near future we plan to revise the model of chapter 2 where the secondary-electrons are not considered to be cold any more.

Chapter 4

Conclusion and future work

In this thesis the influence of secondary-electrons on the stability of the presheath was investigated using both theory (section 2) and particle simulations (section 3). Secondary-electrons are emitted from the wall due to the impact of primary particles. They get accelerated by the sheath potential and enter the presheath as a fast beam where they may induce the corresponding electron-beam instability.

The calculation of the theoretical part refers to the collisional presheath. The sheath influences the presheath solution by imposing the appropriate boundary conditions at the sheath-presheath boundary. Three particle species are considered: ions, primary electrons and cold secondary-electrons. Secondary-electrons enter the presheath with a velocity equal or higher than the plasma electron thermal velocity. At the sheath-presheath boundary also quasineutrality and the Bohm criterion are prescribed. First the stationary state solution is found (section 2.3). The following main calculation includes the derivation of the dispersion relation (section 2.4). The numerical solution of the dispersion relation shows that an instability induced by the secondary electrons can be expected.

Particle-in-cell (PIC) simulations showed (in accordance with theory) no change of the basic plasma parameters with changing secondary electron emission coefficient in the presheath . In the sheath we observed a dependence of the potential drop on the secondary electron emission coefficient which is in very good agreement with theoretical results [5]. Only with respect to the secondary-electron-velocity theory and simulation show qualitative disagreement which we account to the instability induced by the secondary-electrons. The instability induced by the secondary electrons could be clearly demonstrated in the frequency spectrum of the potential. Identical simulations

performed with four times more particles confirmed that the observed instability does not have numerical reasons.

In addition to these already known [18] results we propose a mechanism responsible for the saturation of the instability. Examining the simulations we observed that the temperature of the initially cold secondary-electrons increases in the direction away from the wall. As a consequence the secondary-electron-velocity distribution flattens leading to a shallower minimum of the total-electron-velocity distribution. When the minimum is shallow enough the Penrose criterion is not fulfilled any more and the instability saturates.

To confirm the proposed saturation mechanism future investigations will include an appropriate theory treating the secondary-electrons not any more as cold. Additional simulations will be performed with secondary-electrons having a finite temperature directly after their generation at the wall.

List of Symbols

For the list of symbols $*$ is an abbreviation of an arbitrary string.

$e_{x/y/z}$	unit vectors in x, y and z direction, respectively
B	magnetic field
c_S	ion sound velocity, $c_S = \sqrt{(k_B T_i + k_B T_e)/m_i}$
$\frac{D}{Dt}$	convective derivative $\frac{D}{Dt} = \frac{\partial}{\partial t} + v \cdot \frac{\partial}{\partial x} + a \cdot \frac{\partial}{\partial v}$
e	elementary charge, $e = 1.6022 \cdot 10^{-19} C$
γ	secondary electron emission coefficient
Γ	particle flux $\Gamma(x) = n(x)u(x)$
j	current density
k_B	Boltzmann constant, $k_B = 1.38 \cdot 10^{-23} JK^{-1}$
M	ion velocity relative to the ion sound velocity, $M = u_i/c_S$
ν_*	collision frequency
n_e	electron density
n_i	ion density
n_n	density of neutrals
n_{se}	density of secondary electrons
N	number of simulation particles
N_c	number of spatial grid cells
N_t	number of simulation time steps
ϕ	potential
q	charge of a particle
ρ	charge density
σ_*	collision cross section
u_e	electron velocity
u_i	ion velocity
u_{se}	velocity of secondary electrons
v	velocity as variable or velocity of a particle
v_{th}	thermal velocity of electrons, $v_{th} = \sqrt{k_B T_e/m_e}$
ω_c	cyclotron frequency, $\omega_c = eB/m_e$
ω_p	plasma frequency, $\omega_p = \sqrt{ne^2/\epsilon_0 m_e}$

List of Figures

List of Tables

Bibliography

[1] C.K. Birdsall and A.B. Langdon 1985. Plasma physics via computer simulation. McGraw-Hill Book Company.

[2] T.J.M. Boyd and J.J. Sanderson 2002. The Physics of Plasmas. Cambridge University Press.

[3] F.F. Chen 1984. Plasma physics and controlled fusion. Vol1: plasma physics. Plenum Press, New York.

[4] G. Eibl 1997. Diploma thesis: Numerische Verfahren zur Berechnung von Lösungszweigen nichtlinearer Gleichungssysteme.

[5] G.D. Hobbs and J.A. Wesson 1967. Heat flow through a Langmuir sheath in the presence of electron emission. Plasma Physics, 9, 85-87.

[6] S. Kuhn and M. Hörhager 1986. External-circuit effects on Pierce-diode stability behavior. J. Appl. Phys., 60, 1952-59.

[7] S. Kuhn 1994. The physics of bounded plasma systems (BPS's): Simulation and interpretation. Contrib. Plasma Phys., 34 (4), 495-538.

[8] A.B. Mikhailovskii 1974. Theory of plasma instabilities, Vol.1: Instabilities of a homogeneous plasma. Consultants Bureau, New York, London.

[9] A. Ostermann. Lecture "Numerische Lösung gewöhnlicher Differentialgleichungen"

[10] S.V. Patankar 1980. Numerical heat transfer and fluid flow.

[11] W. Pfendt 1991. Diploma thesis "Zur analytischen Beschreibung des schwach nichtlinearen Verhaltens der Pierce-Diode". Institute of Theoretical Physics, University Innsbruck.

[12] A. Quayyum et al. 2003. Electron emission and molecular fragmentation during hydrogen and deuterium ion impact on carbon surfaces. J. Nucl. Mat. 313-316.

[13] K.-U. Riemann 2000. Theory of the plasma-sheath transition. J. Tech. Phys., 41 (1), Special Issue, 89-121.

[14] R. Schrittwieser winter semester 2002/2003 Lecture about plasma diagnostics

[15] P.C. Stangeby 2000. The plasma boundary of magnetic fusion devices Institute of Physics Publishing, Bristol and Philadelphia

[16] T. Takizuka and H. Abe 1977. A binary collision model for plasma simulation with a particle code J. Comput. Phys., 25, 205-219.

[17] E.W. Thomas 1984. Secondary electron emission. Nucl. Fusion, Data Compendium for Plasma-Surface Interactions, Special Issue

[18] D. Tskhakaya and S. Kuhn 2000. Influence of secondary electrons on the stability of the plasma-wall transition, 2000 International Congress on Plasma Physics (ICPP) combined with the 42^{nd} APS-DPP-Meeting, Quebec City, Canada, 23-27 Oct 2000, Vol.1, 89-92. Bull.APS 45 (7), 334, Abstr. VP1 27.

[19] D. Tskhakaya and S. Kuhn, 2002. Effect of E×B Drift on the Plasma Flow at the Magnetic Presheath Entrance. Contrib. Plasma Phys., 42 (2-4), 302-308.

[20] D. Tskhakaya and S. Kuhn 2002. Particle simulations of the magnetized hydrogen plasma-wall transition taking into account collisions with hydrogen. 29th Conference on Plasma Phys. and Contr. Fusion Montreux, 17-21 June 2002 ECA Vol.26B, P-2.094.

[21] V. Vahedi and M. Surendra 1995. A Monte Carlo collision model for the particle-in-cell method: applications to argon and oxygen discharges Comp. Phys. Com., 87, 179-198.

[22] J.P. Verboncoeur, M.V. Alves, V. Vahedi and C.K. Birdsall 1993. Simultaneous potential and circuit solution for 1D bounded plasma particle simulation codes Journal of computational physics, 104, 321-328.